A control-oriented approach to estimate the injected fuel mass on the basis of the measured in-cylinder pressure in multiple injection diesel engines

A CONTROL-ORIENTED APPROACH TO ESTIMATE THE INJECTED FUEL MASS ON THE BASIS OF THE MEASURED IN-CYLINDER PRESSURE IN MULTIPLE INJECTION DIESEL ENGINES

*Roberto Finesso, Ezio Spessa**

IC Engines Advanced Laboratory, Politecnico di Torino

c.so Duca degli Abruzzi 24, 10129 - Torino, Italy

Key Words: diesel, control-oriented, injection, pilot, main

ABSTRACT

A new control-oriented methodology has been developed to estimate the injected fuel quantities, in real-time, in multiple injection DI diesel engines on the basis of the measured in-cylinder pressure.

The method is based on the inversion of a predictive combustion model that was previously developed by the authors, and that is capable of estimating the heat release rate and the in-cylinder pressure on the basis of the injection rate. The model equations have been rewritten in order to derive the injected mass as an output quantity, starting from use of the measured in-cylinder pressure as input.

It has been verified that the proposed method is capable of estimating the injected mass of pilot pulses with an uncertainty of the order of ±0.15 mg/cyc, and the total injected mass with an uncertainty of the order of ±0.9 mg/cyc. The main sources of uncertainty are related to the estimation of the in-cylinder heat transfer and of the isentropic coefficient $\gamma=c_p/c_v$.

The estimation of the actual injected quantities in the combustion chamber can represent a

*Corresponding Author: Tel. +39-011.090.4482; Fax: +39-011.090.4599; e-mail: ezio.spessa@polito.it

powerful means to diagnose the behavior of the injectors during engine operation, and offers the possibility of monitoring effects, such as injector ageing and injector coking, as well as of allowing an accurate control of the pilot injected quantities to be obtained; the latter are in fact usually characterized by a large dispersion, with negative consequences on the combustion quality and emission formation.

The approach is characterized by a very low computational time, and is therefore suitable for control-oriented applications.

NOMENCLATURE

A: heat transfer area

AC: Alternating Current

B: Bore diameter

BDC: Bottom Dead Center

BMEP: Brake Mean Effective Pressure

BTDC: Before Top Dead Center

c: coefficient of sensitivity

CA: crank angle

c_0: Woschni heat transfer calibration coefficient

CLD: Chemi-Luminescence Detector

c_p: specific heat at constant pressure

c_v: specific heat at constant volume

DI: Direct Injection

DoE: Design of Experiment

DT: Dwell Time

ECU: Electronic Control Unit

EGR: Exhaust Gas Recirculation

EOC: End of Combustion

EOI: End of Injection

ET: Energizing Time

EVO: Exhaust Valve Opening

GMPT-E: General Motors PowerTrain-Europe

h: heat transfer convective coefficient

H_L: lower heating value of the fuel

HLM: HRR local minima criterion to estimate the SOC of intermediate pulses

HRR: Heat Release Rate

ICEAL-PT: Internal Combustion Engine Advanced Laboratory at the Politecnico di Torino

IMEP: Indicated Mean Effective Pressure

IVC: Intake Valve Closing

k: coverage factor

K: combustion rate parameter of the heat release model

m: compression phase polytropic coefficient; mass

$\dot{m}_{f,inj}$: fuel injection rate

MFB50: crank angle at which 50% of the fuel mass fraction has burned

n: engine speed

NEDC: New European Driving Cycle

p: pressure

PCCI: Premixed Charge Compression Ignition

p_f: injection pressure

PFP: Peak Firing Pressure

p_{int}: intake manifold pressure

p_m: motored pressure

q: generic injected fuel quantity [mm^3]

$q_{f,inj}$: total injected fuel quantity [mm^3]

$q_{pil,tot}$: total injected fuel quantity of the pilot pulses [mm^3]

Q: energy

Q_{ch}: released chemical energy

Q_{fuel}: chemical energy of the injected fuel

Q_{ht}: heat exchanged by the charge with the walls

$Q_{ht,glob}$: heat globally exchanged by the charge with the walls over the combustion period

Q_{net}: net energy

R: gas constant

R^2: squared correlation coefficient

RAFR: relative air-to-fuel ratio

RMSE: root mean square of the error

SOC: Start of Combustion

SOI: Start of Injection

S_p: *Mean piston speed*

t: time

T: temperature

TAF: time average filtering

T_{int}: intake manifold temperature

T_{SOI}: temperature evaluated at SOI

T_w: wall temperature

TDC: Top Dead Center

u^2 : variance

U: Expanded uncertainty

V: volume

V_d: cylinder displacement

WG: wastegate

Greek Simbols

$\gamma = c_p/c_v$: isentropic coefficient

ρ: density

ρ_{SOI}: density evaluated at SOI

τ: ignition delay parameter of the heat release model

Subscripts

exp: experimental

f, inj: injected fuel

f, evap: evaporated fuel

glob: global

ht: heat transfer

inj: injected

int: related to the intake manifold

main: related to the main injection

pil: related to the pilot injection

Superscripts

SOC: calculated from the start of combustion

Notation

*: constant in time

1. INTRODUCTION

Modern DI diesel engines usually adopt multiple injections in order to optimize pollutant formation, combustion noise and efficiency [1-3]. The injected fuel quantity of each pulse is usually set by the ECU (Electronic Control Unit) in open-loop control mode, on the basis of an injector map; this map usually provides the injected quantity as a function of the energizing time (ET) (i.e., the duration of the electric command provided to the injector) and of the injection pressure (p_f), and is derived from an experimental steady-state characterization of the injectors performed at the hydraulic test bench [4, 5]. However, a real-time control of the actual injected quantities has not yet been developed. The actual quantity of fuel that is injected into the combustion chamber can in fact be very different from that resulting from the steady-state injector map, as a consequence of several effects. First, the dynamic pressure effects that are induced in the pipes by multiple injection strategies may lead to a variability of the actual injected quantities even for a constant ET, depending on the time interval between consecutive injections (i.e., on the dwell-time DT) and on the injection pressure [4, 5]. Moreover, effects such as injector ageing and coking [6] may lead to a worsening of the injection system performance, which cannot currently be predicted by ECUs.

A critical situation occurs for pilot injections, in which the injected quantity is very small. The actual amount of injected fuel mass of the pilot pulses may in fact be highly dispersed during engine operation, and this may depend on the injection parameters (i.e., DT, p_f) or on injection system ageing. Considering that pilot pulses affect pollutant formation [2, 7], and above all soot formation [8] to a great extent, it could be very useful to be able to perform real-time diagnostics of the actual injected fuel mass in the combustion chamber during engine operation in order to improve the combustion quality and to reduce engine-out pollutant emissions.

Interest in control-oriented predictive combustion models that simulate the heat release rate and in-cylinder pressure in diesel engines has been growing over the last few years, due to their good predictive capability and the increasing computational performance of modern ECUs [9-17]. One of the most widely adopted methods used to simulate the heat release in DI diesel engines is the accumulated fuel mass approach [11-17]. This method is based on the assumption that the rate of released chemical energy is proportional to the energy associated with the fuel quantity made available for combustion at the considered instant. This energy can be computed at time t as the difference between the chemical energy associated with the injected fuel quantity and the cumulative heat release. The accumulated fuel mass method has the great advantage of being able to directly relate the injection rate to the combustion rate, and is therefore physically consistent. This approach has been applied extensively and successfully to a wide range of engine hardware setups and operating conditions [13-17].

The capability of this model to correctly correlate the injection rate with the heat release rate has suggested the possibility of using the same model to derive the injected fuel mass as an output quantity, starting from the experimental heat release rate that is obtained from the measured in-cylinder pressure. The model equations have therefore been rewritten in order to derive the injected fuel mass as a function of the heat release rate. The proposed methodology therefore requires the measurement of the in-cylinder pressure, which can be carried out by means of pressure sensors embedded in the glow-plugs (e.g., see [18]); these pressure sensors could also be used for closed-loop combustion control tasks as shown in [18].

The investigation has been carried out on a GM 2.0 L diesel engine at several representative key-points of the NEDC (New European Driving Cycle), which feature a pilot-main injection strategy. The approach that is proposed in this study to estimate the actual injected quantities is based on combustion diagnostics; alternative methods based on the measurement of hydraulic variables in the injection system, have already been proposed in the literature, such as those reported in [19-20]. In that study, a miniaturized hot-film anemometer with titanium/platinum metallization was developed on a low-temperature co-fired ceramics substrate and integrated in a Common Rail injection nozzle, so that the injected fluid velocity could be measured. The integration of a ceramic flow sensor chip in the nozzle leads to an additional cost compared to the baseline injector configuration. Moreover, it may cause some disturbances to the fluid properties inside the nozzle and induce a reduction in the injected quantities. However, it offers the advantage of being able to directly monitor the injected fuel velocity in each injector.

The method proposed in the present study is based on the measured in-cylinder pressure. This solution also requires an additional cost, related to the need to install integrated pressure sensors in the cylinders; however, these sensors can also be used for additional tasks, such as closed-loop combustion control of combustion phasing. An advantage of the proposed method is that it does not cause disturbances in the fluid properties inside the nozzle; however, a limit in the minimum dwell-time between consecutive injections is introduced, as the method assumes that any heat release overlapping between consecutive injection pulses is negligible.

In the present investigation, a comparison was made between the injected quantities that are predicted by the model and those which are derived from the ECU on the basis of the injector map. The total injected quantity predicted by the model was also compared with that derived from a fuel flow meter. The investigation was carried out on some representative operating conditions of the NEDC.

A sensitivity analysis on the effects of the main model parameters was also carried out, and the uncertainty of the estimated injected quantities was evaluated.

Finally, an analysis of the required computational time was also done.

2. TEST ENGINE AND EXPERIMENTAL SETUP

The model has been assessed and applied to a Euro 5 GMPT-E 2.0 L engine equipped with a twin-stage turbocharger and with piezo-driven injectors. The main engine specifications are reported in Table 1.

Table 1 – Main specifications of the Euro 5 diesel engine.

Engine type	2.0L "Twin-Stage" Euro 5
Displacement	1956 cm^3
Bore x stroke	83.0 mm x 90.4 mm
Connecting rod length	145 mm
Compression ratio	16.5
Valves per cylinder	4
Turbocharger	Twin-stage with valve actuators and WG
Fuel injection system	Common Rail 2000 bar piezo
Specific power and torque	71 kW/l – 205 Nm/l
Injector specifications	d=137 μm, C_d = 0.8, C_a =0.84, C_v =0.95

The experimental data were acquired in a previous research activity that was financially supported by GMPT-E and which had the aim of investigating the potentialities of innovative piezo- and solenoid-driven Common Rail injection systems on engine performance, emissions, fuel consumption and combustion [3]. The experimental tests, related to the engine and to the injectors, were carried out at the highly dynamic test bed and at the hydraulic test rig at ICEAL-PT (Internal Combustion Engine Advanced Laboratory at the Politecnico di Torino).

The experimental characterization of the injectors was carried out at the Bosch-Moehwald hydraulic bench [4-5], which is instrumented for a complete fluid-dynamic characterization of Common Rail fuel-injection systems, and includes an EVI injection-rate meter, an EMI2 device to gauge the oil injected mass as well as thermo-piezo-transducers to measure temperature and pressure traces in the rail and at the injector inlet.

The engine dynamic test rig was equipped with: an 'ELIN AVL APA 100' cradle-mounted AC dynamometer, featuring a power of 220 kW, a nominal torque of 525 Nm, and a maximum speed of 12000 rpm; an 'AVL KMA 4000' system, used to continuously meter engine fuel consumption; an 'AVL AMAi60' raw exhaust-gas analyzer.

All of the abovementioned measuring instruments were controlled by the AVL PUMA OPEN 1.3.2 automation system. The test bed environment was interfaced with AVL CAMEO software to run intelligent engine calibration procedures on the basis of the DoE (Design of Experiment) approach.

The engine was fully instrumented with piezoresistive pressure transducers and K and T thermocouples to measure the pressure and temperature levels at various engine locations. An 'NGK' UEGO air-fuel ratio sensor was placed inside the exhaust system. A Kistler 6058A41 high-frequency piezoelectric transducer was fitted to the glow-plug seat to measure the in-cylinder pressure time-histories. The in-chamber pressure traces were referenced on the basis of the pressure in the intake manifold, which was measured by means of a high-frequency Kistler 4075A10 piezoresistive transducer. The latter was located at the inlet runner of the cylinder equipped with the in-cylinder pressure sensor.

2.1. Experimental tests

The method was tested on six key-points (expressed in terms of engine speed x BMEP), which were identified in order to characterize the engine operations in a medium-sized passenger car over an NEDC. The key-points are: 1500x2, 1500x5, 2000x2, 2000x5, 2500x8, 2750x12 rpm x bar. Table 2 summarizes the main engine parameters for the six analyzed tests.

Table 2 – Main specifications of the six analyzed key-points.

Key-point	p_f	Intake O_2	p_{int}	q_{pil} (ECU)	$q_{f,inj}$ (ECU)	SOI pil	SOI main
	bar	%	bar	mm^3	mm^3	deg BTDC	deg BTDC
1500x2	458	15.98	0.963	1.7	7.6	10.7	-2.37
1500x5	589	16.73	1.169	1.6	17.3	12.2	-0.75
2000x2	554	16.58	1.051	1.6	9.3	16.2	-0.86
2000x5	753	16.73	1.373	1.4	18.2	17.0	-0.12
2500x8	1198	17.83	2.01	1.2	33.2	25.4	3.84
2750x12	1481	17.69	2.23	1.1	46.7	30.5	6.63

3. DESCRIPTION OF THE COMBUSTION MODEL

A detailed description of the model, including the calibration and validation procedures, has already been given in detail in [13-15]. However, a summary is reported hereafter for the sake of clarity.

The heat release model is based on the accumulated fuel mass approach, which assumes that, at any time instant, the rate of chemical energy released by the fuel is proportional to the energy associated with the in-cylinder accumulated fuel mass. This energy can be calculated at time instant t as the difference between the chemical energy of the injected fuel mass and the released chemical energy.

The released chemical energy $Q_{ch,j}$ at time t, for each pulse j ($1 \le j \le N$) of the injection event, is therefore evaluated as follows:

$$\frac{dQ_{ch,j}}{dt} = K_j \left[Q_{fuel,j}\left(t-\tau_j\right) - Q_{ch,j}\left(t\right) \right] \qquad (1)$$

where K_j and τ_j are model calibration quantities, related to the combustion rate and to the ignition delay, respectively, and $Q_{fuel,j}$ is the chemical energy associated with the injected fuel mass:

$$Q_{fuel,j} = \int_{t_{SOI,j}}^{t} \dot{m}_{f,inj} H_L dt \qquad t \le t_{EOI,j} \qquad (2)$$

$$Q_{fuel,j} = \int_{t_{SOI,j}}^{t_{EOI,j}} \dot{m}_{f,inj} H_L dt \qquad t > t_{EOI,j} \qquad (3)$$

SOI and EOI denote the start and end of injection, respectively, $\dot{m}_{f,inj}$ the injection rate and H_L the lower heating value of the fuel. The total released chemical energy can be calculated as the sum of the contributions of all the injection pulses:

$$Q_{ch} = \sum_{j=1}^{N} Q_{ch,j} \qquad (4)$$

The K_j and τ_j parameters have to be appropriately tuned in order to obtain a good matching between the predicted Q_{ch} curves and those derived from the experimental in-cylinder pressure [13].

The calibration is performed for several steady-state operating conditions, and physically-consistent correlations are then derived as a function of significant engine variables. The tuning procedure of the model for the engine considered in this study is reported in [15].

With reference to the combustion rate coefficients, it was found, in [13-15], that a constant value can be taken for the combustion rate parameter of the pilot pulse (i.e., K_{pil}). Instead, it was shown, in [13-15], that a dependence exists between the combustion rate parameter of the main pulse (i.e., K_{main}) and the engine speed/load conditions, and this dependence can be taken into account either by means of a look-up table or by means of simple correlations such as those shown in [13]. In addition, a reduction factor was introduced in [15] to correctly account for low-density/low-oxygen operating conditions, which may induce a remarkable decrease in the combustion rate.

The ignition delay parameters were studied in detail in [21], and the following correlations were identified for the engine considered in the present study:

$$\tau_{pil} = 0.008977\rho_{SOI}^{2} - 0.36077\rho_{SOI} + 3.8619 \qquad (5)$$

$$\tau_{main} = 3.8E4\,\rho_{SOI}^{-2.2} \exp^{\left(\frac{2100}{T_{SOI}}\right)} O_2^{-1.9}\, p_f^{-0.31} q_{pil,tot}^{-0.35} \qquad (6)$$

Equation (5) indicates that only the charge density calculated at SOI (ρ_{SOI}) is necessary for a good estimation of the ignition delay of the pilot injections, as the physical contribution is predominant over the chemical one [21]. Instead, the effect of the intake charge oxygen concentration (O_2), of the charge density and temperature at SOI (ρ_{SOI}, T_{SOI}), of the injection pressure (p_f) and of the total injected pilot quantity ($q_{pil,tot}$) have to be included to accurately predict the ignition delay of the main pulse.

ρ_{SOI} and T_{SOI} are calculated assuming that the in-chamber thermodynamic conditions at BDC are equal to those in the intake manifold (p_{int}, T_{int}):

$$\rho_{SOI} = \frac{p_{\text{int}}}{RT_{\text{int}}}\left(\frac{V_{BDC}}{V_{SOI}}\right) \qquad (7)$$

$$T_{SOI} = T_{\text{int}}\left(\frac{V_{BDC}}{V_{SOI}}\right)^{m-1} \qquad (8)$$

where *m* is the polytropic coefficient during the compression phase.

The choice of using BDC as the reference angle to estimate ρ_{SOI} and T_{SOI} is just a convention. It was in fact verified that the values of ρ_{SOI} and T_{SOI} obtained using, for example, IVC as the reference crank angle are very similar (i.e., the root mean square difference is of the order of 0.34 kg/m^3 and 5.3 K, respectively, for the key-points analyzed in the present paper).

The values of ρ_{SOI} and T_{SOI} obtained using Eq. (7) and Eq. (8) are obviously approximations of the actual values inside the combustion chamber. The actual values of ρ_{SOI} could be estimated by dividing the total trapped mass by the in-chamber volume at SOI. The total trapped mass is the sum of the trapped air mass, of the trapped EGR mass and of the residual gas mass. The different contributions could be evaluated on the basis of the air-to-fuel ratio and of the EGR rate, which can in turn be estimated with the procedure shown in [22]. The actual T_{SOI} values could instead be evaluated by applying the ideal gas law at SOI, using the values of the in-cylinder pressure at SOI and of the total trapped mass.

Figure 1a shows a comparison between the actual values of ρ_{SOI} and those obtained using Eq. (7), while Fig. 1b shows a comparison between the actual values of T_{SOI} and those obtained using Eq. (8), for the key-points analyzed in the present study.

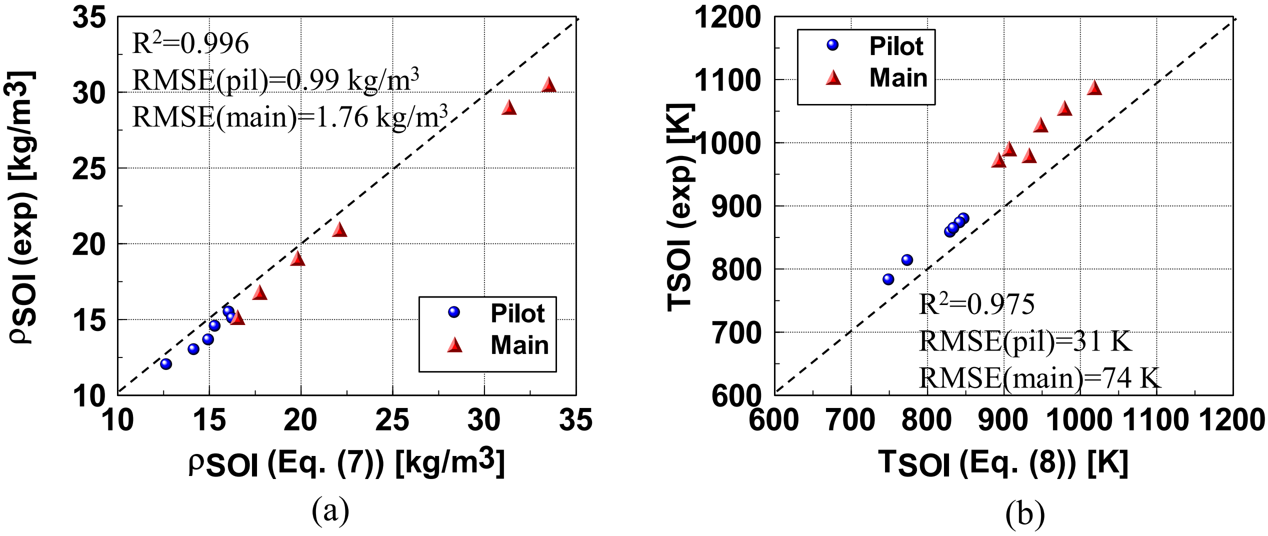

Figure 1 – Experimental vs. calculated values of ρ_{SOI} using Eq. (7) (a); experimental vs. calculated values of T_{SOI} using Eq. (8) (b).

In general, the approximation of the density is quite good, as the average root mean square (RMS) difference is 0.99 kg/m^3 for the $\rho_{SOI,pil}$ term and 1.76 kg/m^3 for the $\rho_{SOI,main}$ term (the use of Eq. (7) leads to an overestimation). With reference to T_{SOI}, it can be seen that the average root mean square difference between the values obtained with Eq. (8) and the actual ones are 31 K for $T_{SOI,pil}$ and 74 K for $T_{SOI,main}$. The underestimation obtained using Eq. (8) is mainly due to the heat transfer effects during the intake phase and to the residual gas contribution being neglected. Moreover, the greater overestimation of $T_{SOI,main}$ is due to the charge heating caused by the pilot combustion being neglected.

However, it can be seen, in Fig. 1, that the use of Eqs. (7-8) allows the trends of ρ_{SOI} and T_{SOI} to be captured, so that the differences, with respect to the true values, are indirectly taken into account through the tuning of the exponents in Eqs. (5-6). Moreover, Eqs. (7-8) require the intake manifold pressure and temperature, which are known quantities for the ECU, as input, and they can therefore be considered suitable for control-oriented applications.

O_2 can be derived from the real-time EGR and intake charge model [23], while p_f and $q_{pil,tot}$ are known quantities for the engine ECU.

The predicted released chemical energy Q_{ch} can be used as a starting quantity to evaluate the charge net energy (i.e., Q_{net}) which is given, at each time instant, by the difference between the released chemical energy and the heat exchanged by the charge with the walls, i.e., Q_{ht} [24]:

$$Q_{net} = Q_{ch} - Q_{ht} \qquad (9)$$

Q_{net} can be approximated by means of a uniform scaling of the Q_{ch} curve, according to the procedure proposed in [13-15]; the scaling factor includes the global heat exchanged between the charge and the walls over the combustion period, i.e., $Q_{ht,glob}$.

The net energy of the charge can therefore be approximated as follows [13]:

$$Q_{net}^{SOC} \cong Q_{ch} \frac{m^*_{f,inj} H_L - Q_{ht,glob}}{m^*_{f,inj} H_L} \qquad (10)$$

where $m^*_{f,inj}$ is the total injected fuel mass and H_L the lower heating value of the fuel; the superscript (SOC) indicates that Q_{net} is evaluated from the start of combustion onwards. The $Q_{ht,glob}$ parameter must be known in order to apply Eq. (10). In general, it is necessary to derive a physically consistent correlation for this parameter, such as that proposed in [13], as a function of the ratio between the injected fuel quantity and the engine speed. The experimental values of $Q_{ht,glob}$, which are necessary to identify this correlation, are calculated as the difference between the chemical energy of the total injected mass (i.e., $m^*_{f,inj} H_L$) and the value of the experimental net energy curve evaluated at the end of combustion. The experimental net energy curve ($Q_{net,exp}^{SOC}$) can be derived from the measured in-cylinder pressure using a single zone approach [24]:

$$dQ_{net,exp}^{SOC} = \frac{\gamma}{\gamma - 1} p_{exp} dV + \frac{1}{\gamma - 1} V dp_{exp} \qquad (t \geq t_{SOC}) \qquad (11)$$

where $\gamma = \frac{c_p}{c_v}$ is the ratio of the specific heats, and was evaluated as a function of the relative air-to-fuel ratio, according to the correlation that was proposed in [13]:

$$\gamma = -0.0064 RAFR^2 + 0.0563 RAFR + 1.2151 \qquad (12)$$

The experimental values of γ used to derive Eq. (12) are shown in Fig. 2, and were derived in [13] for a 1.9L GM diesel engine using different values of the compression ratio. The values of the squared correlation coefficient R^2 and of the root mean square error (RMSE) for the predicted vs. experimental values of γ are also reported in the chart.

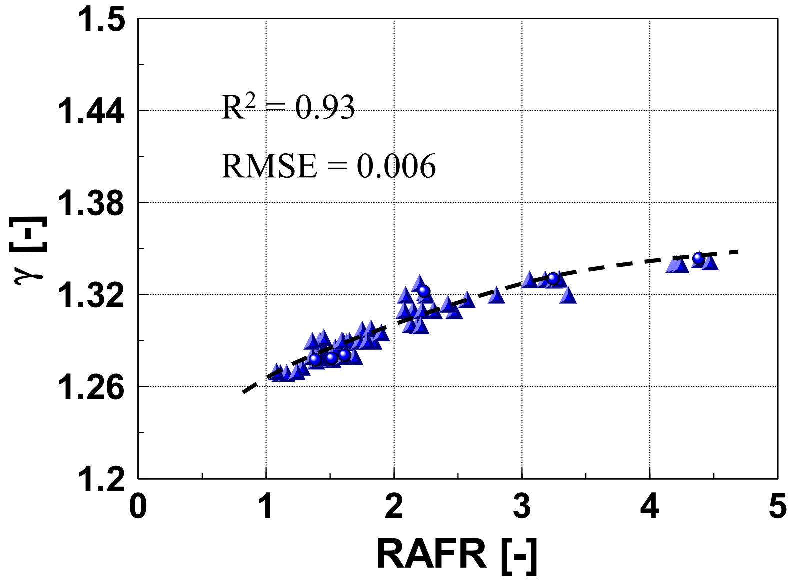

Figure 2– Trend of the experimental values of the γ parameter as a function of the relative air-to-fuel ratio [13].

The experimental value of $Q_{ht,glob}$ is therefore calculated as follows:

$$Q_{ht,glob,exp} = m^*_{f,inj} H_L - Q^{SOC}_{net,exp}(t_{EOC}) \qquad (13)$$

It is convenient to use an accurate estimate of the total injected mass in Eq. (13) (e.g., that derived from a fuel flow meter) in order to accurately evaluate the global heat transfer parameter. The calibration of the $Q_{ht,glob}$ parameter was carried out in [13-15] using the values of the fuel flow rate that were measured by means of a fuel flow meter installed at the test bed; this flow rate was split into equal parts over the 4 cylinders, and converted into an average injected mass per cycle. It has in fact been verified that, for the present engine, the performance of the four injectors is similar (see section 3.1).

It was found in [13-15] that $Q_{ht,glob}$ is well correlated with the $q_{f,inj}/n$ parameter, where $q_{f,inj}$ indicates the total injected quantity of fuel and n the engine speed. The following correlation was derived from engine map tests acquired on a GM 1.9L diesel engine with a similar hardware setup to that of the present study, but equipped with solenoidal injectors (see [14]):

$$Q_{ht,glob} = 7656 \cdot \frac{q_{f,inj}\left[mm^3\right]}{n\left[rpm\right]} + 14.4 \;\; J \qquad (14)$$

Figure 3 shows the experimentally-derived values of $Q_{ht,glob}$ that were used to identify Eq. (14) (blue triangles), as well as the experimentally-derived values of $Q_{ht,glob}$ for the six key-points considered in this study (red circles). It can be noted that the values of the key-points are in trend.

The values of the squared correlation coefficient R^2 and of the root mean square error (RMSE) for the predicted vs. experimental values of $Q_{ht,glob}$ are also reported in the chart.

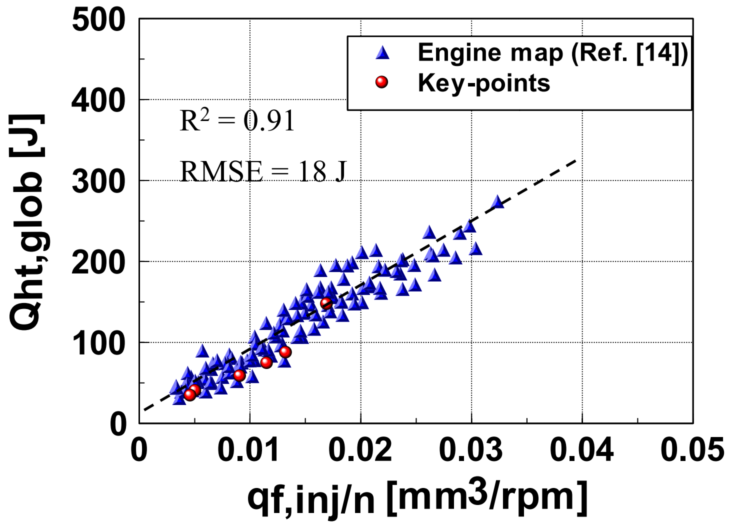

Figure 3 – Trend of the experimental values of the $Q_{ht,glob}$ parameter, as a function of the qf,inj/n quantity, for the engine map tests of ref [14] and for the key-points of the present study.

It will be shown, in Section 5, that a correct estimation of this parameter is fundamental in order to accurately predict the injected fuel quantities.

The estimation of the net energy of the charge, i.e., Q_{net}, allows the in-cylinder pressure to be predicted in the interval between SOC and EOC, using a single zone approach, as follows:

$$dp = \left(\frac{\gamma - 1}{V}\right)\left(dQ_{net} - \frac{\gamma}{\gamma - 1}\, pdV\right) \qquad (15)$$

The reconstruction of the complete in-cylinder pressure trace also includes the compression and expansion phases, which are modeled by means of polytropic evolutions, and the gas exchange phases, which are modeled as constant pressure evolutions (see [13-15]). In particular, the following correlations were used to estimate the polytropic coefficients of the compression and expansion phases:

$$m = 0.0011\, q_{f,inj}(mm^3) + 1.30 \qquad (16)$$

$$m' = -0.0016\, q_{f,inj}(mm^3) + 1.38 \qquad (17)$$

3.1 Analysis of the cylinder-to-cylinder dispersion of the injectors

Although only a single cylinder was instrumented for the pressure measurements, the cylinder-to-cylinder dispersion of the injectors installed on the present engine was verified indirectly on the basis of the analysis of the measured gas temperatures in the four exhaust runners. In general, the temperatures of the exhaust gases outflowing from each cylinder depend on combustion phasing (related to the injection phasing), on the air-to-fuel ratio (related to the injected fuel quantity) and on heat transfer effects in the cylinders and in the runners. Outer cylinders are in general characterized by higher heat transfer rates than inner ones.

Figure 4 reports the values of the exhaust gas temperatures in the four runners (Fig. 4a), as well as the differences between the temperatures of the cyl1-cyl4 and cyl2-cyl3 exhaust runners (Fig. 4b).

It can be noted that the outer cylinders are characterized by systematically lower temperatures than the inner ones, due to a higher heat transfer rate. However, by comparing the temperatures of the outer cylinders (cyl1, cyl4), as well as those of the inner cylinders (cyl2, cyl3), it can be noted that the differences are small (i.e., of the order of 5-10°C)

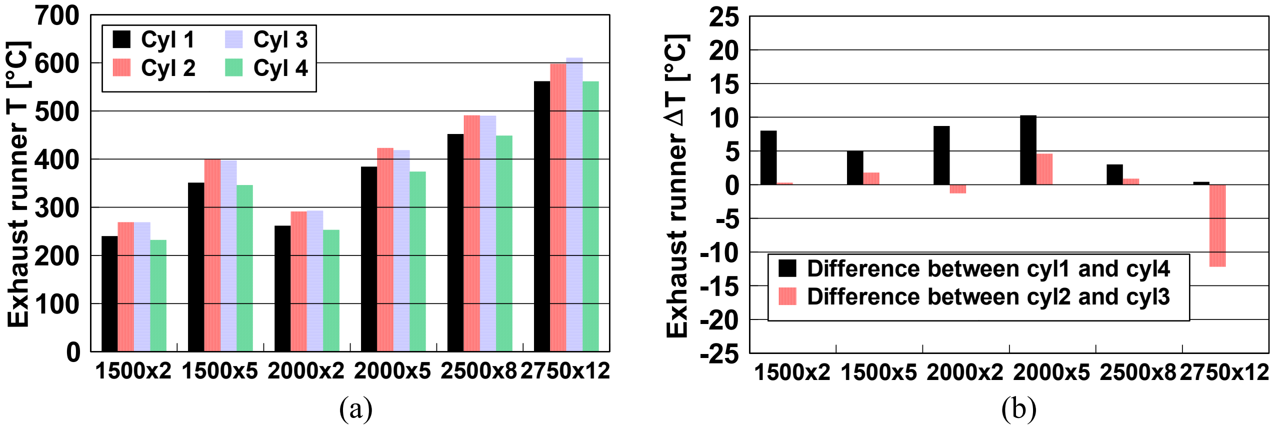

Figure 4 – Values of the gas temperatures in the exhaust runners of the four cylinders (a); differences between the temperatures of the gases in the cyl1 and cyl4 exhaust runners, as well as between the cyl2 and cyl3 ones (b).

This indirectly confirms that the behavior of the injectors installed in cyl1 and cyl4, as well as of those installed in cyl2 and cyl3, is very similar in terms of injection phasing and total injected quantity. In order to verify this, the combustion model was applied to the six key-points to test the impact of a deviation of ±2 deg in the injection phasing of the main pulse, as well as of a deviation ±1 mg in the injected quantity, on the predicted in-cylinder temperatures at EVO. The results are shown in Tab. 3.

Table 3 – Impact of variations in SOI_{main} and in the injected fuel mass on T_{EVO}, using the combustion model

Key-point	SOI_{main}+2deg	SOI_{main}-2deg	$m_{f,inj}$+1mg	$m_{f,inj}$-1mg
	ΔT_{EVO} [°C]	ΔT_{EVO} [°C]	ΔT_{EVO} [°C]	ΔT_{EVO} [°C]
1500x2	-4.6	5.3	36.8	-37.5
1500x5	-7.7	8.6	26.9	-27.0
2000x2	-6.0	6.5	37.0	-37.8
2000x5	-8.6	9.2	25.5	-26.2
2500x8	-10.5	11.3	18.1	-18.2
2750x12	-13.6	14.5	15.5	-15.6

It can be noted that the experimental differences in the exhaust gas temperatures shown in Fig. 4b correspond to a lower dispersion of the injected quantities than 1 mg/cyc for the same SOI_{main}, or to a lower dispersion of SOI_{main} than 2 deg for the same $m_{f,inj}$.

Moreover, in a recent research activity devoted to the refinement of the combustion model [17], each cylinder of a 1.6L GM engine has been instrumented with pressure transducers. It has been verified that the average cylinder-to-cylinder dispersion of IMEP was of the order of 0.6 bar (corresponding to a dispersion of the total injected quantity of about 0.5 mg/cyc), and that the average cylinder-to-cylinder dispersion of MFB50 was of the order of 0.5 deg. This confirms that the injector dispersion in modern diesel engines is very low.

4. ESTIMATION OF THE INJECTED MASS ON THE BASIS OF THE MEASURED IN-CYLINDER PRESSURE

The combustion model inversion procedure, which allows the injected fuel mass to be calculated as a model output, starting from the measured in-cylinder pressure time-histories, is reported hereafter.

A pilot-main injection strategy has been considered for the development of the method, which is however of general application. It has been assumed that the dwell-time between consecutive injections is not too short, so as to prevent overlapping of the heat release contributions that stem from the different injection pulses.

The dwell time threshold generally depends on the specific engine operating condition. In order to give some general indications, a dwell-time sweep was simulated using the combustion model for the six key-points. A threshold was identified for each key-point, under which a significant overlapping of heat release occurs between the pilot and main pulses. The thresholds are reported in Tab. 4.

Table 4 – Estimated dwell-time threshold necessary to avoid significant overlapping between the pilot and main heat release

	DT Threshold [μs]
1500x2	300
1500x5	400
2000x2	500
2000x5	500
2500x8	600
2750x12	600

Starting from Eq. (1), the $Q_{fuel}(t-\tau_j)$ term is made explicit as a function of $Q_{ch,j}$ for each injection pulse j, as follows:

$$Q_{fuel,j}\left(t-\tau_j\right)=Q_{ch,j}\left(t\right)+\frac{1}{K_j}\frac{dQ_{ch,j}}{dt}(t) \qquad (18)$$

It is therefore necessary to obtain an experimental estimation of the $Q_{ch,j}$ curve for each injection pulse in order to evaluate the $Q_{fuel}(t-\tau_j)$ term. The estimation can be made as follows.

First, Eq. (11) is applied to evaluate the whole trend of the experimental charge net energy (i.e., $Q_{net,exp}^{SOC}$) on the basis of the measured in-cylinder pressure.

The calculation is performed from SOC to EOC (a conventional EOC angle, e.g., 430°, can be assumed). The estimation of SOC is therefore necessary; this can be done according to the procedure illustrated in [21].

Once the estimation of $Q_{net,exp}^{SOC}$ has been carried out, the experimental trend of the released chemical energy (i.e., $Q^{SOC}_{ch,exp}$) is drawn by scaling the $Q^{SOC}_{net,exp}$ curve as follows:

$$Q^{SOC}_{ch,exp} \cong Q^{SOC}_{net,exp} \frac{Q^{SOC}_{net,exp}(t_{EOC}) + Q_{ht,glob}}{Q^{SOC}_{net,exp}(t_{EOC})} \qquad (19)$$

This is the inverse procedure to that used to estimate the Q_{net} curve on the basis of the Q_{ch} curve predicted by the combustion model (see Eq. (10)). The $Q_{ht,glob}$ parameter was introduced in Eq. (10) and represents the heat globally exchanged between the charge and the walls during combustion; it can be evaluated through Eq. (14), which was derived from experimental tests.

As an example, Fig. 5 reports, for the 1500x5 key-point, the experimental Q_{net} curve (dotted red line) and the experimental Q_{ch} curve obtained with Eq. (19) (black line). The $Q_{ht,glob}$ parameter is also indicated in the figure. In addition, the experimental Q_{ch} curve obtained using a detailed heat transfer model is also reported with a blue chain line.

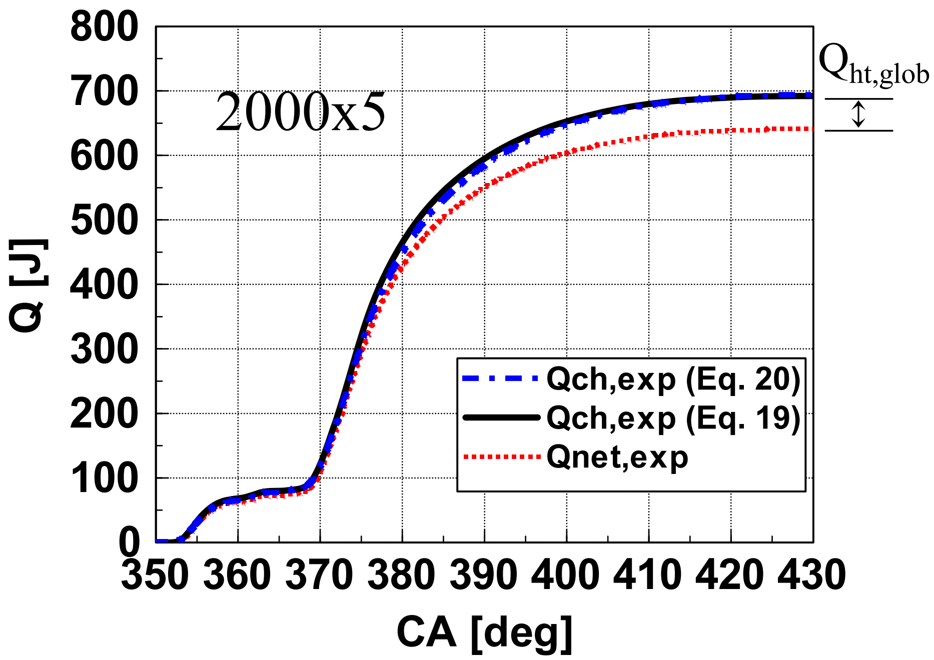

Figure 5 – Trends of the experimental net and chemical energy release for the 2000x5 key-point. The chemical energy release curves obtained from Eq. (19) and using a detailed heat transfer model (Eq. (20)) are reported.

The detailed heat transfer model is based on a convective formula [25]:

$$\dot{Q}_{ht} = hA\left(T - T_w\right) \qquad (20)$$

where h is the convective heat transfer coefficient, A is the instantaneous heat transfer area, T is the instantaneous gas temperature and T_w is the wall temperature.

The convective heat transfer coefficient h [W/m^{2}K] was modeled using the Woschni correlation [26]:

$$h[W/m^2K] = c_0 B[m]^{-0.2} p[bar]^{0.8} T[K]^{-0.53} w[m/s]^{0.8} \qquad (21)$$

$$w = \left[c_1 S_p[m/s] + c_2 \frac{V_d[m^3] T_r(IVC)}{p_r(IVC) V_r[m^3](IVC)} \left(p - p_m\right) \right] \qquad (22)$$

where B is the bore diameter, S_p is the mean piston speed, V_d is the cylinder displacement, while T_r, p_r and V_r represent the in-cylinder temperature, pressure and volume at the moment of intake valve closure, respectively. c_0 was used as a calibration factor, while c_1 and c_2 were kept constant and equal to nominal values of 0.0039 and 2.31, respectively.

It can be observed, in Fig. 5, that the simplified procedure used to estimate Q_{ch} (i.e., Eq. (19)) leads to a good approximation of that obtained with the detailed heat transfer model (i.e., using Eq. (20)), even though a slight overestimation occurs for intermediate CA values between SOC and EOC. Similar trends were obtained for the other key-points, but the results are not reported here for the sake of brevity.

The approach based on the detailed heat transfer model requires the estimation of the instantaneous in-cylinder temperature, which is evaluated through the ideal gas law, using the measured in-cylinder pressure and the total trapped mass in the cylinder as input data. The latter quantity includes the contributions of air, EGR and residual gas.

This approach requires a higher computational time effort than the simplified approach (i.e., Eq.

(19)), and computational time is a critical parameter for control-oriented applications.

Once the $Q_{ch,exp}^{SOC}$ curve has been evaluated, it is necessary to split this curve into the single contributions that stem from each injection pulse. As previously stated, it is assumed that consecutive injections are scheduled using a moderately long dwell-time, in order to reduce the overlapping of the heat release contributions that stem from the different pulses.

First, it is necessary to identify the SOC of each injection pulse. This can be done by means of the methods reported in [21]. The overall SOC (i.e., that of the most advanced injection pulse) is evaluated as the crank angle at which the first chemical energy fraction is released. The SOC of the subsequent injection shots is detected by identifying the relative minima of the HRR curve. This procedure is referred to as the "HRR local minima" (HLM) method.

At this point, the experimental chemical energy release of the different injection pulses j (i.e., $Q_{ch,j,exp}$, where j ranges from 1 to N, 1 indicates the most advanced pulse and N indicates the most delayed one) can be calculated as follows. With reference to the most advanced pulse (i.e., j=1):

$$\begin{aligned} Q_{ch,1,exp} &= Q_{ch,exp}^{SOC} \quad (t_{SOC} \leq t < t_{SOC,2}) \\ Q_{ch,1,exp} &= Q_{ch,exp}^{SOC}(t_{SOC,2}) \quad (t \geq t_{SOC,2}) \end{aligned} \tag{23}$$

where SOC is the overall start of combustion and SOC,2 is the SOC of the second injection pulse.

The contribution of the chemical energy release of the subsequent pulses, excluding the last one (i.e., 2≤j≤N-1), is instead calculated as follows:

$$\begin{aligned} Q_{ch,j,exp} &= Q_{ch,exp}^{SOC} - Q_{ch,exp}^{SOC}(t_{SOC,j}) \quad (t_{SOC,j} \leq t < t_{SOC,j+1}) \\ Q_{ch,j,exp} &= Q_{ch,exp}^{SOC}(t_{SOC,j+1}) - Q_{ch,exp}^{SOC}(t_{SOC,j}) \quad (t \geq t_{SOC,j+1}) \end{aligned} \tag{24}$$

Finally, the contribution of the chemical energy release of the most delayed pulse (i.e., j=N), is derived as follows:

$$Q_{ch,N,exp} = Q^{SOC}_{ch,exp} - Q^{SOC}_{ch,exp}(t_{SOC,N}) \qquad (t_{SOC,N} \leq t \leq t_{EOC}) \qquad (25)$$

The procedure is illustrated in Fig. 6 for the 2000x5 key-point featuring a pilot-main injection strategy.

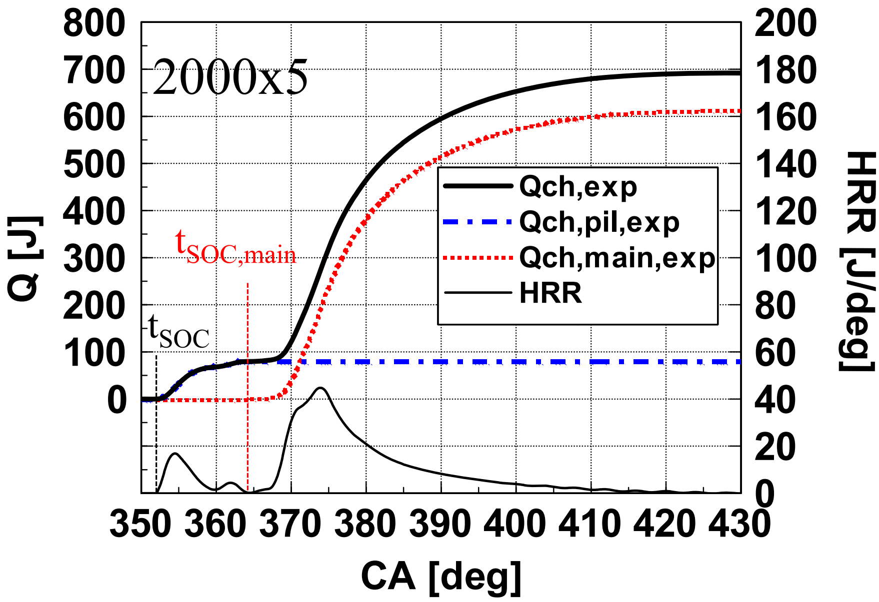

Figure 6 – Trends of the global experimental chemical energy release and contributions of the pilot and main injections evaluated with Eqs. (23-25) for the 2000x5 key-point. The trend of HRR is also reported.

Figure 6 reports the overall experimental chemical energy curve (thick black line), as well as the contributions of the pilot (blue chain line) and main (pointed red line) pulses evaluated by means of Eqs. (23-25). The SOC instants evaluated with the above-mentioned procedures are also indicated, as is the HRR curve (thin black line).

The $Q_{fuel,j}$ term can now be estimated at time t through the following equation, which is derived from Eq. (18) taking the τ_j parameter into account:

$$Q_{fuel,j}(t) = Q_{ch,j}\left(t+\tau_j\right) + \frac{1}{K_j}\frac{dQ_{ch,j}}{dt}\left(t+\tau_j\right) \qquad (26)$$

The τ_j parameters are estimated by means of Equations (5-6); when input variables related to the injected quantities are used in the correlations to evaluate the model parameters (i.e., τ_j), the values derived from the injector maps can be used, to avoid iterative procedures; it was in fact verified that the resulting error in the evaluation of the ignition delay parameters is negligible.

The injected fuel mass curve of each injection pulse j can be estimated as follows:

$$m_{f,inj,j} = \frac{Q_{fuel,j}}{H_L} \qquad (27)$$

Finally, the total injected quantity of each pulse can be estimated evaluating the steady-state final value of the injected mass curve evaluated by means of Eq. (27).

The overall injected fuel mass curve, i.e., $m_{f,inj}$, is obtained by summing the contributions of all the injection pulses:

$$m_{f,inj} = \sum_{j=1}^{N} m_{f,inj,j} \qquad (28)$$

Figure 7 shows a scheme that summarizes the proposed methodology.

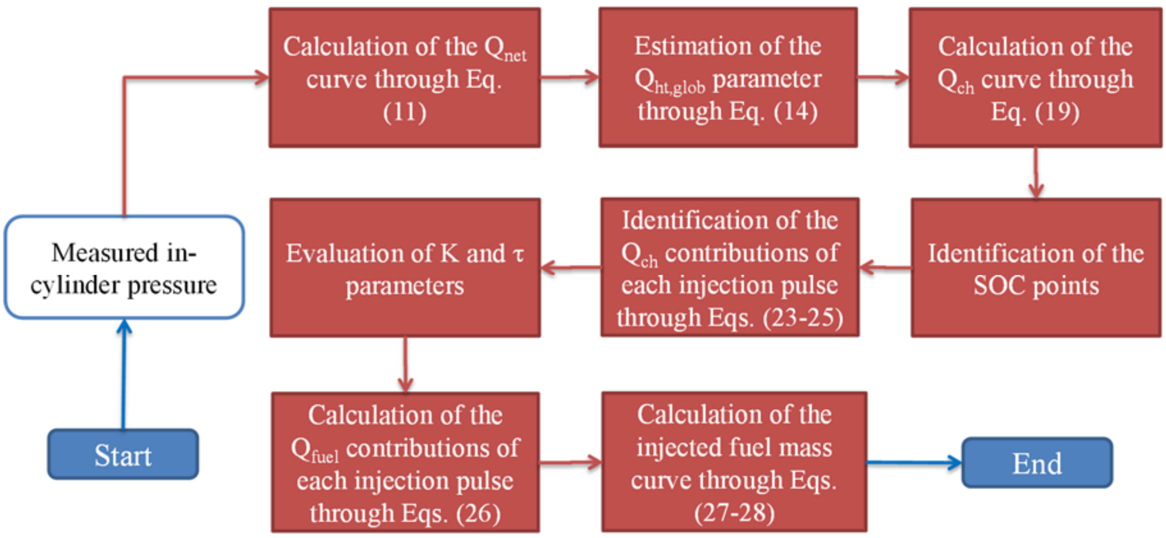

Figure 7 – Scheme of the proposed methodology.

5. RESULTS AND DISCUSSION

The procedure explained in Section 4 was applied to the six key-points whose specifications are reported in Tab. 2. In particular, a comparison was made between the injected fuel mass estimated by means of the proposed method and those derived from the injector map; moreover, a sensitivity analysis was carried out on the main model parameters, and the uncertainty of the pressure-derived values of the injected fuel mass was evaluated.

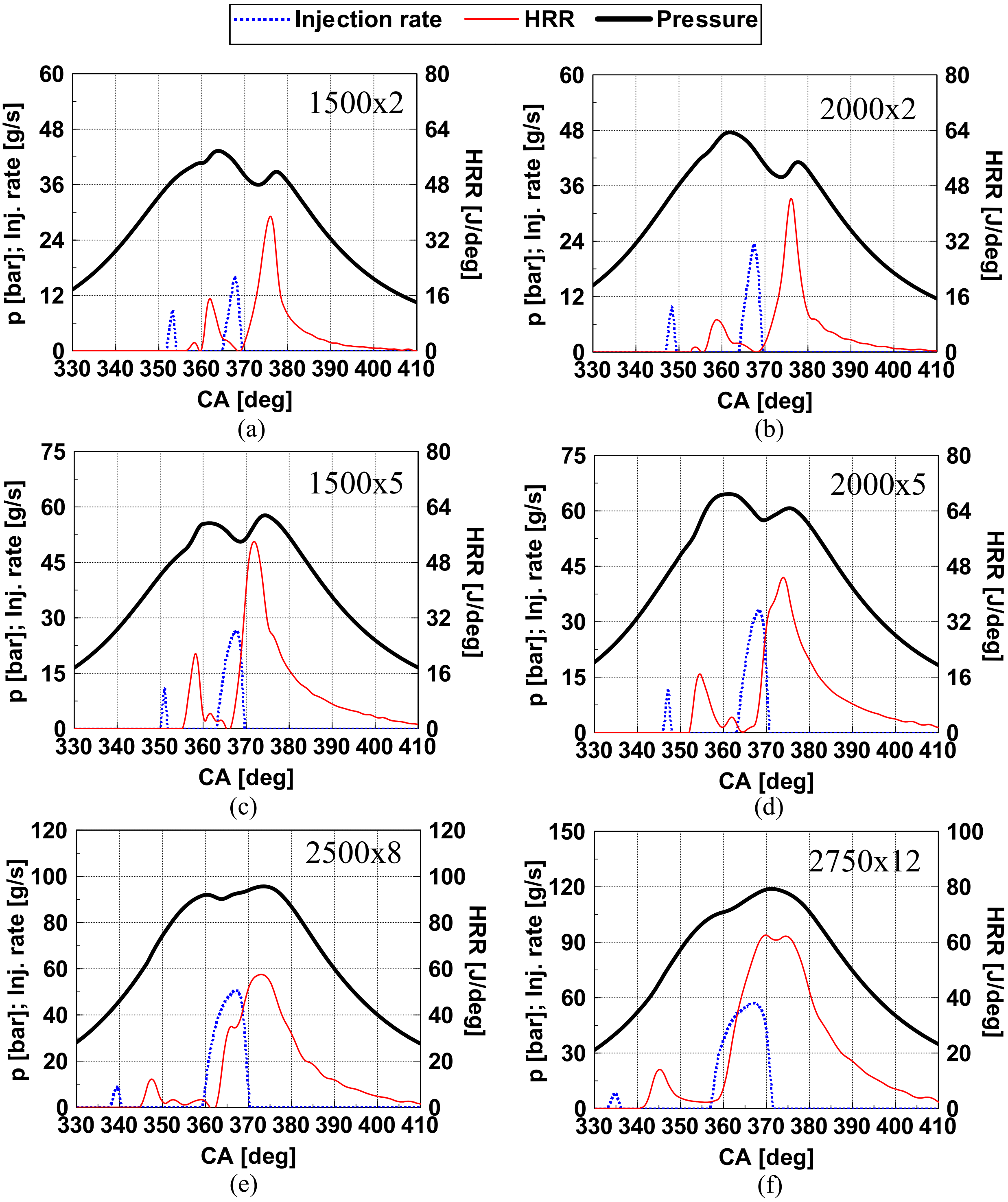

Figure 8 – Trends of the measured in-cylinder pressure, of the pressure-derived HRR and of the injection rate, for the six key-points.

Figure 8 reports the measured in-cylinder pressure trends (black lines), the HRR curves derived from the pressure traces using a single-zone model (thin red lines) and the injection rate profiles (pointed blue lines) for the six key-points. The in-cylinder pressure traces shown in Fig. 8 were obtained as the average of 100 consecutive cycles, which were filtered using the TAF (Time-average filtering) procedure shown in [27]. This procedure is based on the following steps. First, the time average of the instantaneous pressure is evaluated in the discrete consecutive CA intervals into which the engine cycle is divided, and the resulting averaged pressure values, taken in the middle of the respective intervals, are interpolated through cubic spline fitting to obtain the original in-cylinder pressure curve.

It can be noted, in Fig. 8, that all the key-points feature a pilot-main injection strategy. Moreover, it can be observed, from the HRR traces, that the 1500x2, 2000x2 and 1500x5 key-points show dominant premixed combustion, while the remaining key-points show a premixed-mixing controlled combustion type. It can be noted that HRR premixed and mixing controlled combustion peaks for the latter key-points are of the same order of magnitude, due to the adoption of a pilot injection which leads to a reduction in the premixed combustion contribution. A single injection strategy would lead to much higher HRR peaks during the premixed combustion phase.

With reference to the model outcomes, Figure 9a reports, for the six key-points, the values of the pressure-derived total injected fuel mass, as well as the values obtained from the injector map and those derived from the fuel flow meter, while Fig. 9b reports the differences between the values obtained from the injector map/fuel meter and those derived from the measured pressure. Figure 9c, instead, reports the values of the pressure-derived pilot injected quantities as well as those derived from the injector map, while Fig. 9d shows the differences between the values obtained from the injector map and those derived from the measured in-cylinder pressure. Figures 6b-d also report the average uncertainty bands of the proposed method. The procedure to estimate the uncertainty is explained in Section 5.2.

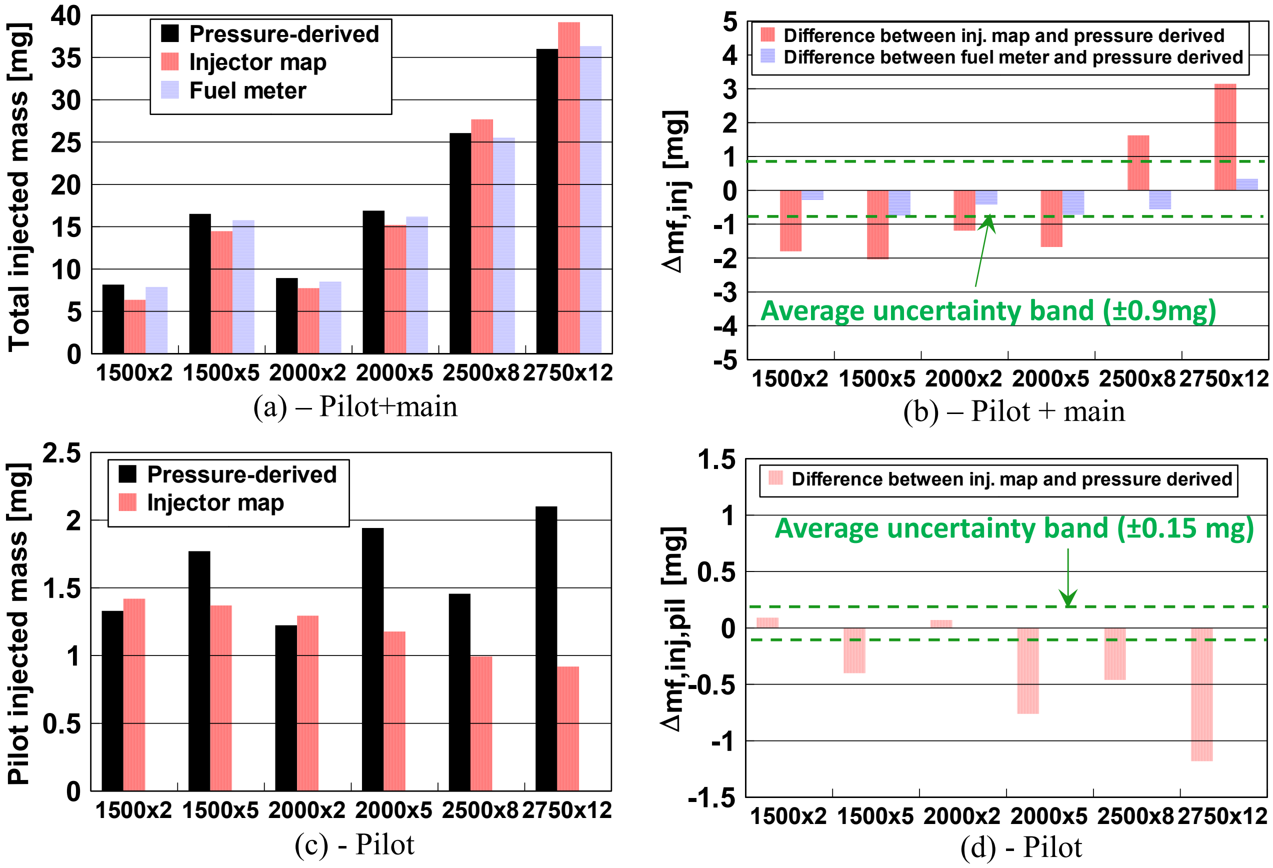

Figure 9 – Comparison between the total (a) and pilot (c) fuel injected quantities derived from the in-cylinder pressure and those derived from the injector map (total, pilot) and fuel meter (total); difference between the injected quantities from the injector maps/fuel meter and those obtained from the in-cylinder pressure (b, d). The average uncertainty bands in the estimation of the pressure-derived injected quantities are also reported.

First, it can be noted that the average uncertainty in the evaluation of the injected mass of the pilot pulses is very small (Fig. 9d), as it is of the order of 0.15 mg. The average uncertainty in the evaluation of the total injected quantity is instead of the order of 0.9 mg, and it will be shown, in Section 5.2, that this value mainly depends on the uncertainty in the evaluation of the heat transfer parameter ($Q_{ht,glob}$) when Eq. (14) is used.

From the results reported in Fig. 9a-b, it can be observed that the pressure-derived total injected quantities are comparable with those derived from the fuel meter, as the difference is below the uncertainty band of the method. It can also be noted that the proposed method diagnoses several deviations in the total injected quantities estimated by the injector map, (i.e., by the ECU): the quantities of the medium-low load key-points (i.e., 1500x2-5, 2000x2-5) are underestimated, while those of the medium-high load key-points (i.e., 2500x8, 2750x12) are overestimated. In particular, the deviations of the ECU-derived total injected quantities are of the order of +3 mg for the 2750x12 key-point, of +1.7 mg for the 2500x8 key-point, of -1.5 mg for the 1500x2 and 2000x5 key-points and of -2 mg for the 2000x5 key-point. These deviations can be considered significant, compared with the uncertainty of the method.

With reference to the pilot injected quantities, it can be observed that the method diagnoses significant deviations in the quantities evaluated by means of the injector map at the 2750x12 key-point (-1.3 mg), at the 2000x5 (-0.8 mg) key-point, but also at the 1500x5 and 2500x8 operating conditions (about -0.4/-0.5 mg).

5.1 *Sensitivity analysis*

A sensitivity analysis was carried out in order to verify the effect of the main model parameters on the pressure-derived injected quantities. The first three parameters that were considered in this analysis are the values of the K_j coefficients of the combustion model (see Eq. (26)), the value of the isentropic coefficient γ used in Eq. (11) to derive the experimental Q_{net} trace from the in-cylinder pressure and the $Q_{ht,glob}$ parameter used in Eq. (19) to obtain the experimental Q_{ch} trace, starting from the experimental Q_{net} trace; finally, the effect of horizontal and vertical shifts in the in-cylinder pressure trace were also investigated.

Each parameter was varied separately, keeping the remaining ones unchanged. The analysis was made for the all the key-points. Reasonable variation ranges were chosen for the parameters considered in the sensitivity analysis.

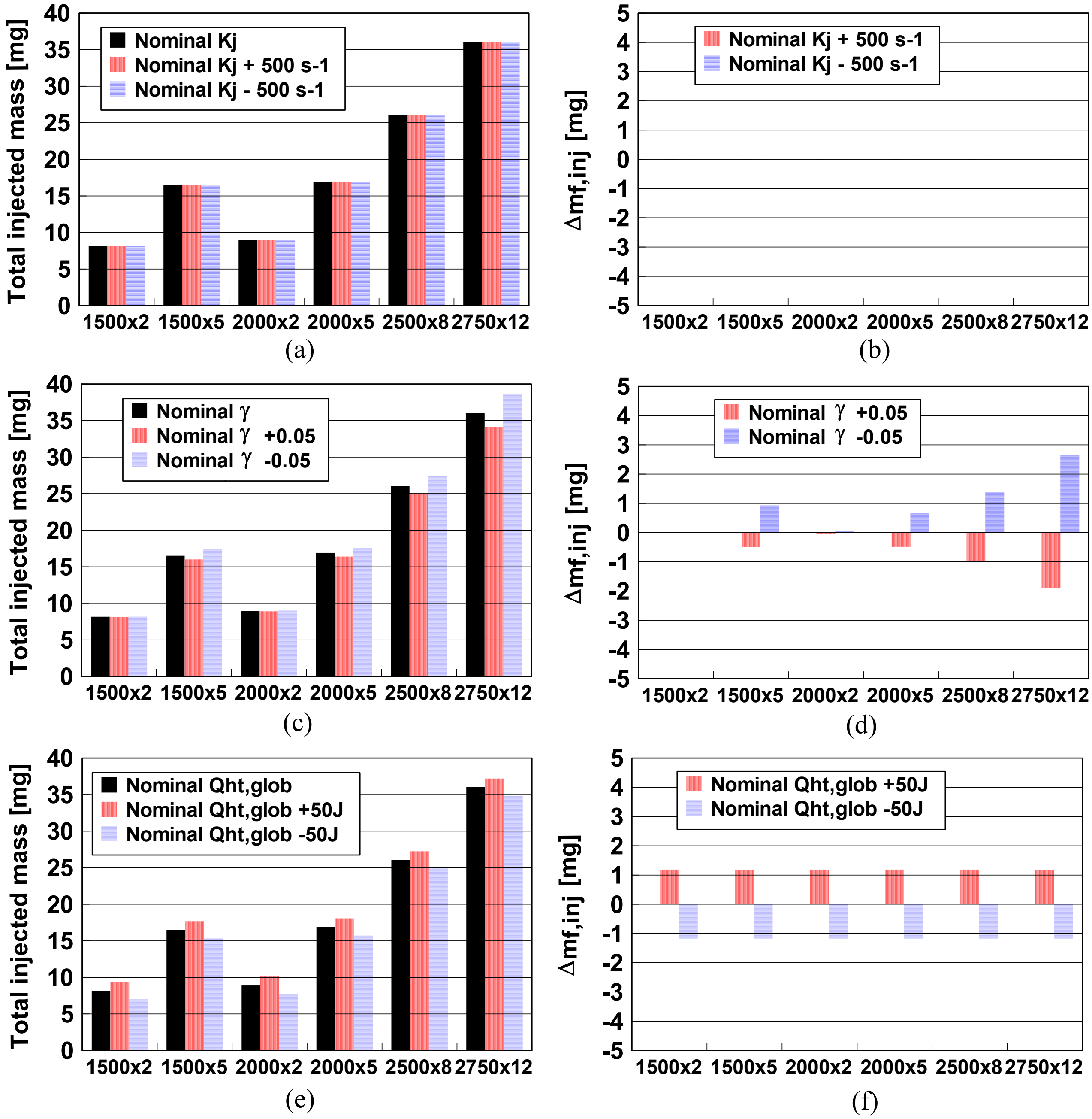

Figure 10 – Effect of a variation in the values of the K_j, γ and $Q_{ht,glob}$ parameters (with respect to the nominal values) on the estimated total injected mass (a, c, e). The differences are also reported (b, d, f).

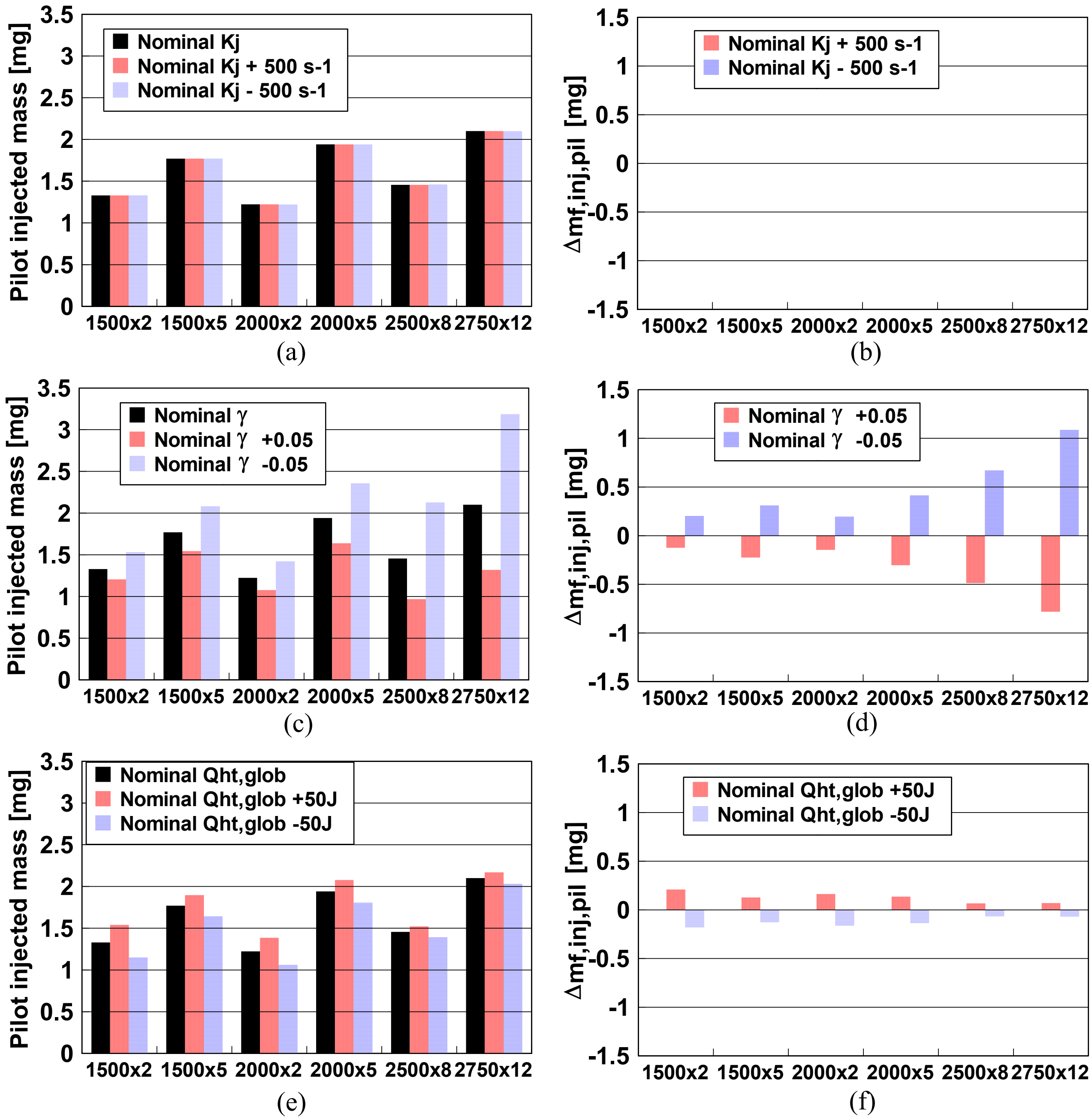

Figure 11 – Effect of a variation in the values of the K_j, γ and $Q_{ht,glob}$ parameters (with respect to the nominal values) on the estimated pilot injected mass (a, c, e). The differences are also reported (b, d, f).

The results are shown in Figs. 10-13. Figures 10-11 report the effect of a variation in the values of the K_j (Figs. 10a, 11a), γ (Figs. 10c, 11c) and $Q_{ht,glob}$ (Figs. 10e, 11e) parameters, with respect to the nominal values, on the estimated total injected quantities (Fig. 10) and pilot injected quantities

(Fig. 11). The differences are also reported in Figs. 10b, 10d, 10f and 11b, 11d,11f.

It can be noted that a variation in the values of the K_j parameter (Figs. 10a,b and 11a,b) does not influence the pressure derived injected quantities to any great extent; a variation in the values of the γ parameter has a remarkable effect on both the pressure-derived total injected quantity (Figs. 10c, d) and on pilot injected quantity (Figs. 11c, d), and the effect increases with the engine load. Finally, it is interesting to note that a variation in the value of $Q_{ht,glob}$ mainly affects the diagnosed total injected quantities (the deviations are independent of the engine load/speed), but has little influence on the diagnosed pilot injected quantities.

This analysis suggests that is important to accurately select the γ parameter to evaluate the charge net energy Q_{net} (see Eq. (11)), as it can significantly affect the estimation of the total and pilot injected quantities. Moreover, a good prediction of the heat transfer parameter $Q_{ht,glob}$ is also required, as it directly affects the estimated total injected quantity. However, the impact of this parameter on the estimated values of the pilot injected quantities can be considered negligible, and this leads to low uncertainty, as will be shown in Section 5.2.

The estimation of the injected quantities could also be affected by an error in the measured in-cylinder pressure trace, which is the main model input. Figures 12-13 report the effect of horizontal and vertical shifts in the in-cylinder pressure trace on the estimated total injected quantities (Fig. 12) and pilot injected quantities (Fig. 13).

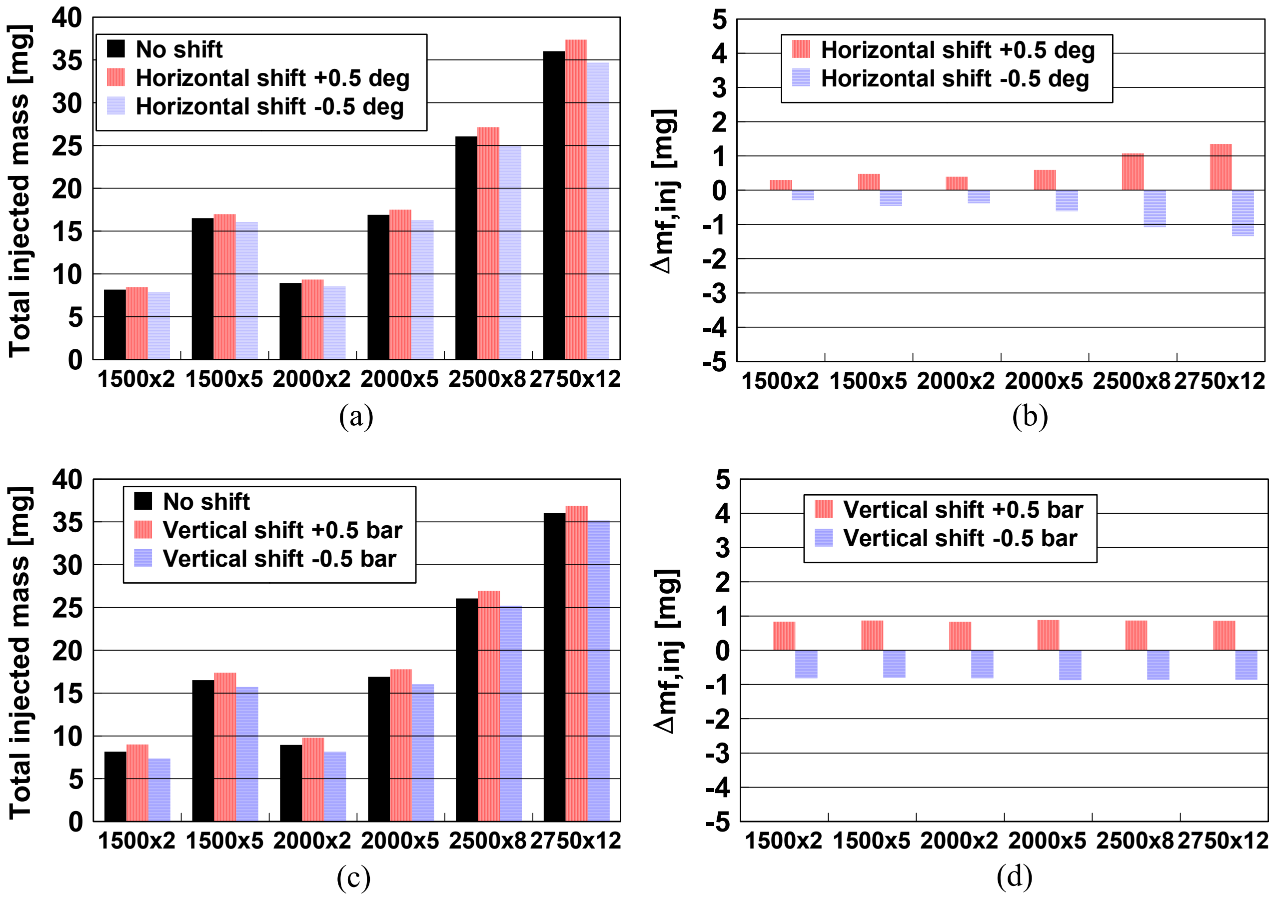

Figure 12 – Effect of a horizontal and vertical shift of the measured pressure on the estimated total injected mass (a, c). The differences are also reported (b, d).

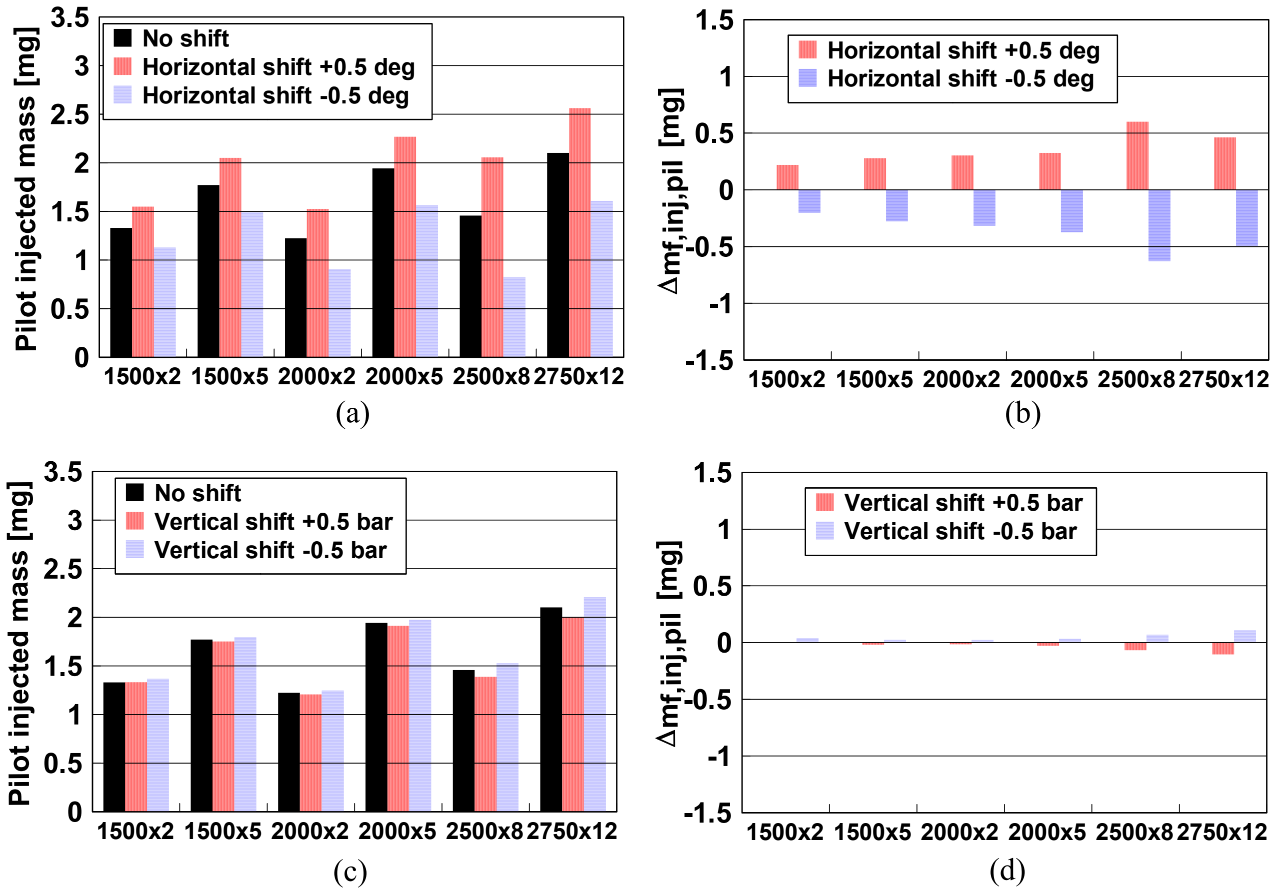

Figure 13 – Effect of a horizontal and vertical shift of the measured pressure on the estimated total injected mass (a, c). The differences are also reported (b, d).

It can be observed, in Fig. 12, that both horizontal and vertical shifts affect the pressure-derived total injected quantities to a great extent, and that the effect of a horizontal shift increases with engine load, while that of a vertical shift is somewhat constant.

With reference to the estimated pilot injected quantities (Fig. 13), it should be noted that a horizontal shift leads to significant deviations, which increase with the engine load, while a vertical shift has little influence.

As a result, attention should be paid to the correct pressure phasing, with respect to the crank angle, and to the correct in-cylinder pressure referencing. The latter may be realized comparing the values of the in-cylinder pressure around BDC with the values measured in the intake manifold by means of an absolute pressure transducer.

5.2 *Evaluation of the experimental uncertainty*

The procedure applied for the evaluation of experimental uncertainties is based on the recommended practices reported in [28] and hereafter summarized.

Given an output quantity *y*, which is dependent on *N* independent x_i variables, the associated variance $u_c^2(y)$ is calculated through the following relation:

$$u_c^2(y) = \sum_{i=1}^{N} \left(\frac{\partial y}{\partial x_i} \right)^2 u^2(x_i) = \sum_{i=1}^{N} c_i^2 u^2(x_i) \qquad (29)$$

Equation (29) is consistent if the mutual effects between independent variables are neglected.c_i is the "coefficient of sensitivity" of the output quantity *y* with respect to the *i-th* independent variable x_i.

Once $u_c^2(y)$ has been evaluated, it is possible, by assuming a level of confidence (e.g., 95%) and a correspondent coverage factor *k* (e.g., equal to 2), to evaluate the expanded combined uncertainty of *y*, $U_c(y)$:

$$U_c(y) = k\sqrt{u_c^2(y)} \qquad (30)$$

If the independent variables x_i are the result of a measurement, the associated variance should be estimated by taking into account the accuracy of the instrument declared in the calibration certificate, the repeatability, the instrument resolution and the master uncertainty.

The procedure was used to estimate the uncertainty in the predicted values of the injected pilot mass and of the total injected quantity for the six analyzed key-points.

The main parameters that could affect the estimation of the injected quantities were identified and analyzed in Section 5.1. However, most of those parameters can be excluded from the uncertainty calculation as they are not sources of error. First, it was shown that the K_j parameters used in the heat release model do not affect the predicted injected quantities to any great extent (see Fig. 10a, 11a). The γ coefficient has remarkable influence on the predicted quantities (see Fig. 10b, 11b), and it should therefore be selected accurately. The correlation developed in [13], as a function of the RAFR parameter, was used in the present study (see Fig. 2 and Eq. (12)). The $Q_{ht,glob}$ parameter also has a significant effect on the estimated total injected quantities (see Fig. 10c) but has little influence on the estimated pilot injected quantities (see Fig. 11c).

Vertical and horizontal shifts in the in-cylinder pressure affect the estimation of Q_{net} and therefore of the pressure-derived injected quantities (see Fig. 11-12). However, if the in-cylinder pressure is referenced correctly (using, for example, an absolute pressure sensor in the intake manifold) and phased correctly (on the basis of the thermodynamic loss angle, see [29]), this error contribution can be excluded from the uncertainty calculation procedure.

The only parameters whose effect on the uncertainty of the method has been considered significant are therefore γ and $Q_{ht,glob}$. These parameters were evaluated, in this study, by means of the correlations expressed in Eq. (12) and Eq. (14), and shown in Fig 2 and Fig. 3, respectively. There are two main sources of error for each of the two parameters; the first one is related to the uncertainty in the input variables that are used in the correlations (i.e., RAFR in Eq. (12), $q_{f,inj}$ and n in Eq. (14)). The second source of error is related to the dispersion of the predicted values of γ and $Q_{ht,glob}$ (through Eq.(12) and Eq. (14), respectively) with respect to the experimental ones; this dispersion was quantified by means of the RMSE parameter, which is equal to 0.006 for the γ parameter and to 18 J for the $Q_{ht,glob}$ parameter, using the proposed correlations. The first source of error was evaluated for each parameter (γ, $Q_{ht,glob}$) by applying Eq. (29) to the analytical expression of γ and $Q_{ht,glob}$ expressed by Eqs. (12, 14), and assuming reasonable values for the variance of the RAFR, $q_{f,inj}$ and n parameters. The second source of error was evaluated on the basis of the RMSE values. However, it has been verified that the first source of error is two orders of magnitude lower than the second one. Moreover, it has also been verified that the contribution of γ is low, compared to that of $Q_{ht,glob}$, but it increases with the engine load (as can also be seen in Figs. 10d, 11d).

Table 5 summarizes the expanded combined uncertainty of the pressure-derived pilot and total injected quantities. It can be noted that the uncertainty in the evaluation of the pilot quantity is very small, as its average is of the order of 0.15 mg. The average uncertainty in the evaluation of the total quantity is instead of the order of 0.9 mg, and is larger at higher engine loads. This uncertainty is mainly related to the dispersion of the predicted values of $Q_{ht,glob}$ by means of Eq. (14), and could be reduced if a more refined method were to be identified to estimate heat transfer.

Table 5 – Evaluation of the expanded uncertainty U of the predicted injected quantities.

Key-point	Pilot	Pilot+main
	mg	mg
1500x2	0.15	0.85
1500x5	0.10	0.87
2000x2	0.15	0.85
2000x5	0.12	0.86
2500x8	0.15	0.90
2750x12	0.24	1.02

5.3 *Analysis of the cycle-by-cycle variations and considerations on the in-cylinder pressure quality*

The proposed methodology has also been tested on single, independent cycles in order to verify its capability of estimating cycle-by-cycle variations in the injected quantities. Moreover, the same analysis has been carried out using the acquired raw pressure, without TAF filtering, in order to verify the effect of signal noise on the outputs. This is an important aspect, as the use of the proposed method in commercial engines would require integrated pressure sensors, which are characterized by a higher signal noise than the Kistler sensor used in the present investigation.

Figures 14-15 report the estimated total and pilot injected quantities, respectively, for 10 consecutive cycles using both filtered and raw pressure, for the six key-points.

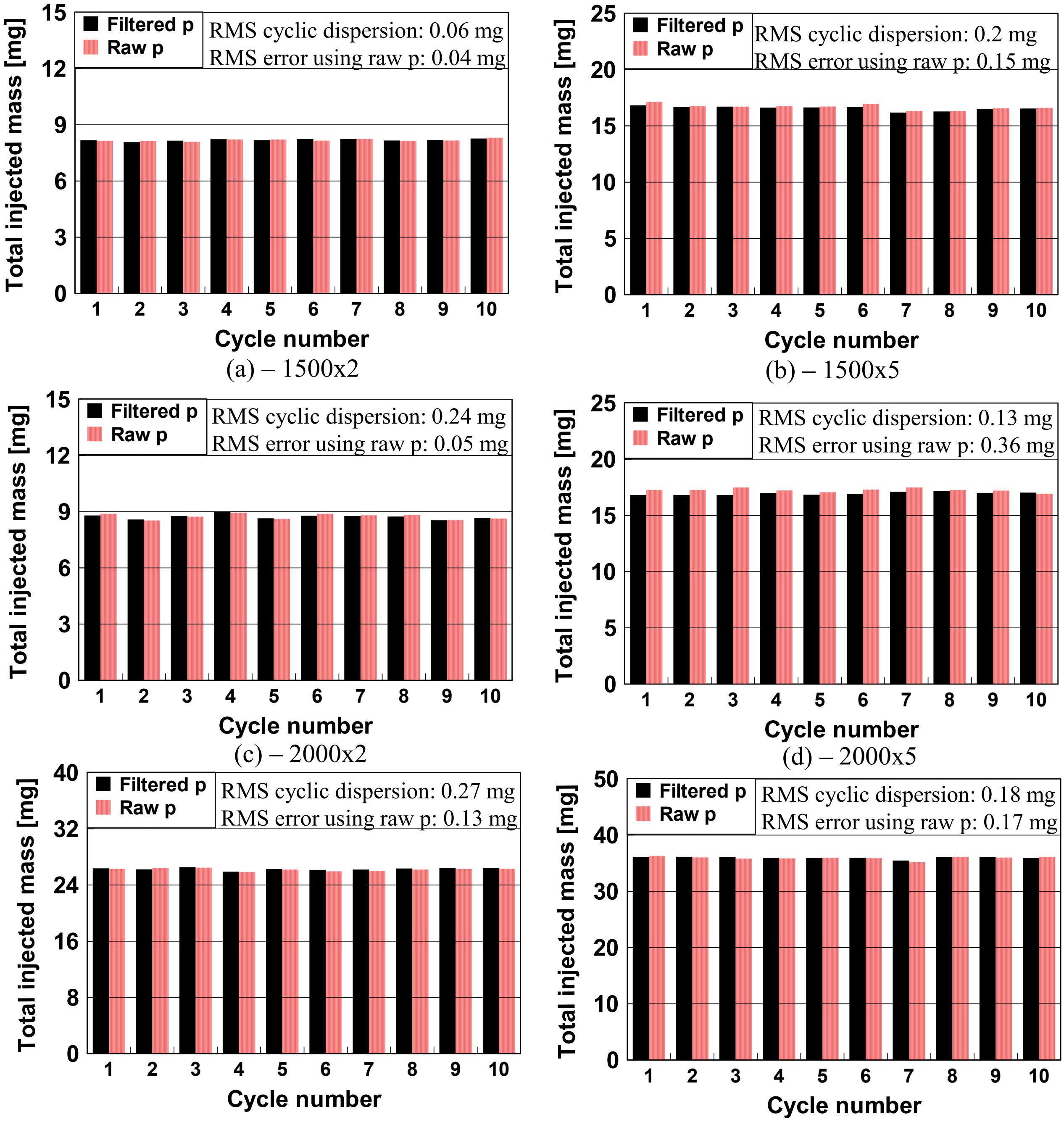

(a) – 1500x2 (b) – 1500x5 (c) – 2000x2 (d) – 2000x5 (e) – 2500x8 (f) – 2750x12

Figure 14 – Estimated total injected quantity for 10 consecutive cycles using both filtered and raw pressure. The RMS cyclic dispersion (calculated using the filtered pressure) and the RMS error of the raw pressure-derived quantities with respect to those

derived from the filtered p are also reported.

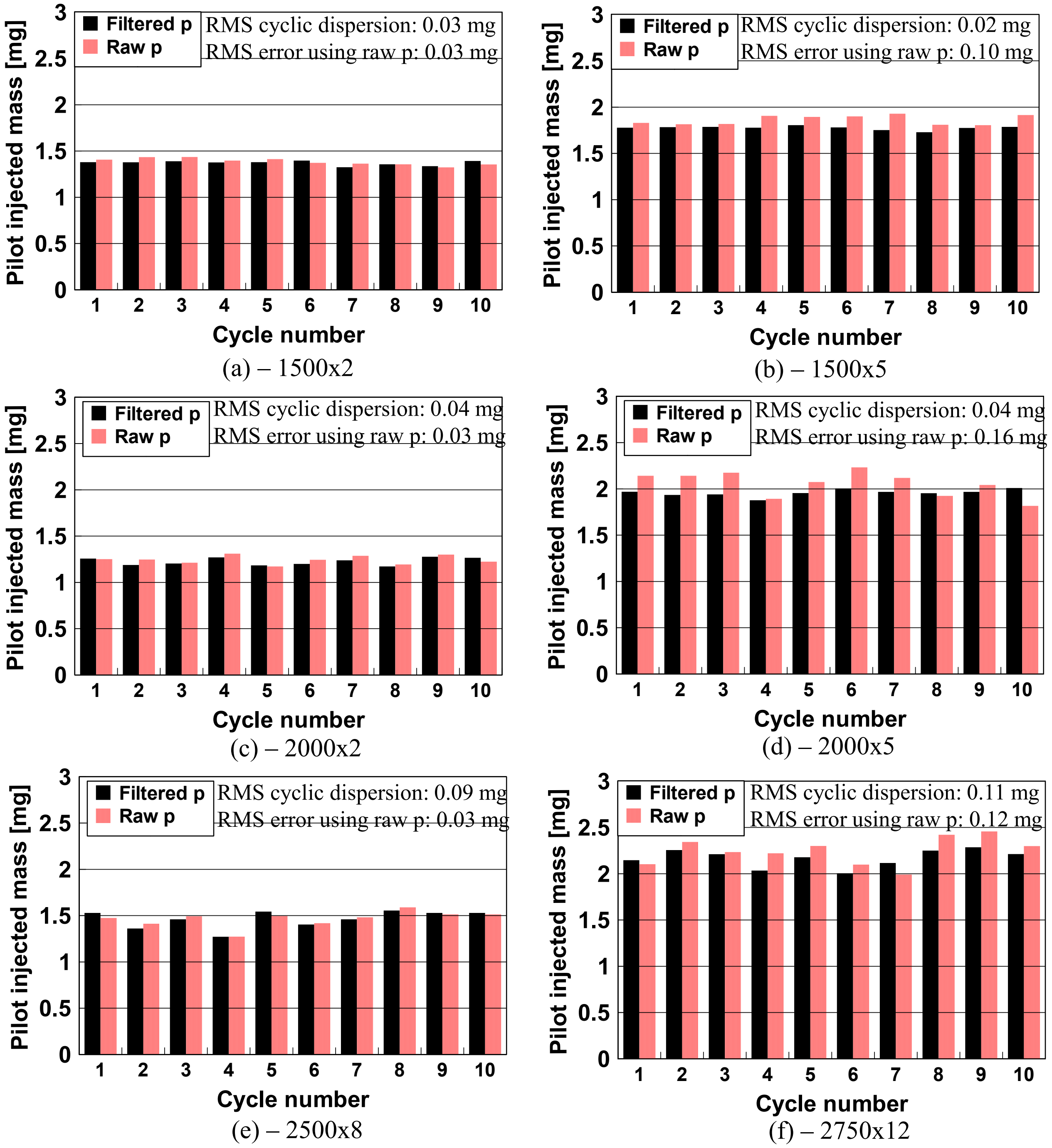

(a) – 1500x2 (b) – 1500x5

(c) – 2000x2 (d) – 2000x5

(e) – 2500x8 (f) – 2750x12

Figure 15– Estimated pilot injected quantity for 10 consecutive cycles using both filtered and raw pressure traces. The RMS cyclic dispersion (calculated using the filtered pressure) and the RMS error of the raw pressure-derived quantities with respect to those derived from

the filtered pressure are also reported.

The RMS cyclic dispersion (calculated using the filtered pressure) and the RMS error of the injected quantities obtained from the raw pressure, with respect to those derived from the filtered pressure, are also reported in the graphs.

It can be noted that, in general, the cycle-by-cycle dispersion of both the pilot and total injected quantities is very low.

The method is also robust with respect to the use of a raw in-cylinder pressure signal. In this case, the errors depend on the specific engine operating conditions. The largest RMS errors occur at the 2750x12 and 2000x5 key-points, and are of the order of 0.36 and 0.17 mg/cyc, respectively, for the main pulse (see Fig. 14) and of the order of 0.12 and 0.16 mg/cycle, respectively, for the pilot pulses (see Fig. 15).

The use of a raw in-cylinder pressure is therefore suitable for estimating average injected quantities for all the operating conditions, while an accurate evaluation of cycle-by-cycle dispersion in general requires filtering of the pressure trace.

5.4 *Analysis of the computational time*

The computational time is basically expected to depend on the crank-angle step used for the in-cylinder pressure; this step should be chosen on the basis of a trade-off between the calculation time and the prediction accuracy.

An analysis has therefore been carried out in order to evaluate the impact of the crank-angle step on the computational time and on the prediction accuracy of the injected fuel quantities.

The elaboration was performed with the Labwindows CVI software, using a Pentium-D

PC.

The effect of the crank-angle step on the average computational time necessary to run a single operating condition is reported in Tab. 6.

Table 6 – Effect of the crank angle step on the computational time.

Calculation step [deg]	0.1	0.5	1.0	2
Computational time: [ms]	3.4	0.9	0.6	0.3

Figure 16, instead, shows the effect of the crank angle step used for integration on the estimated total and pilot injected quantities.

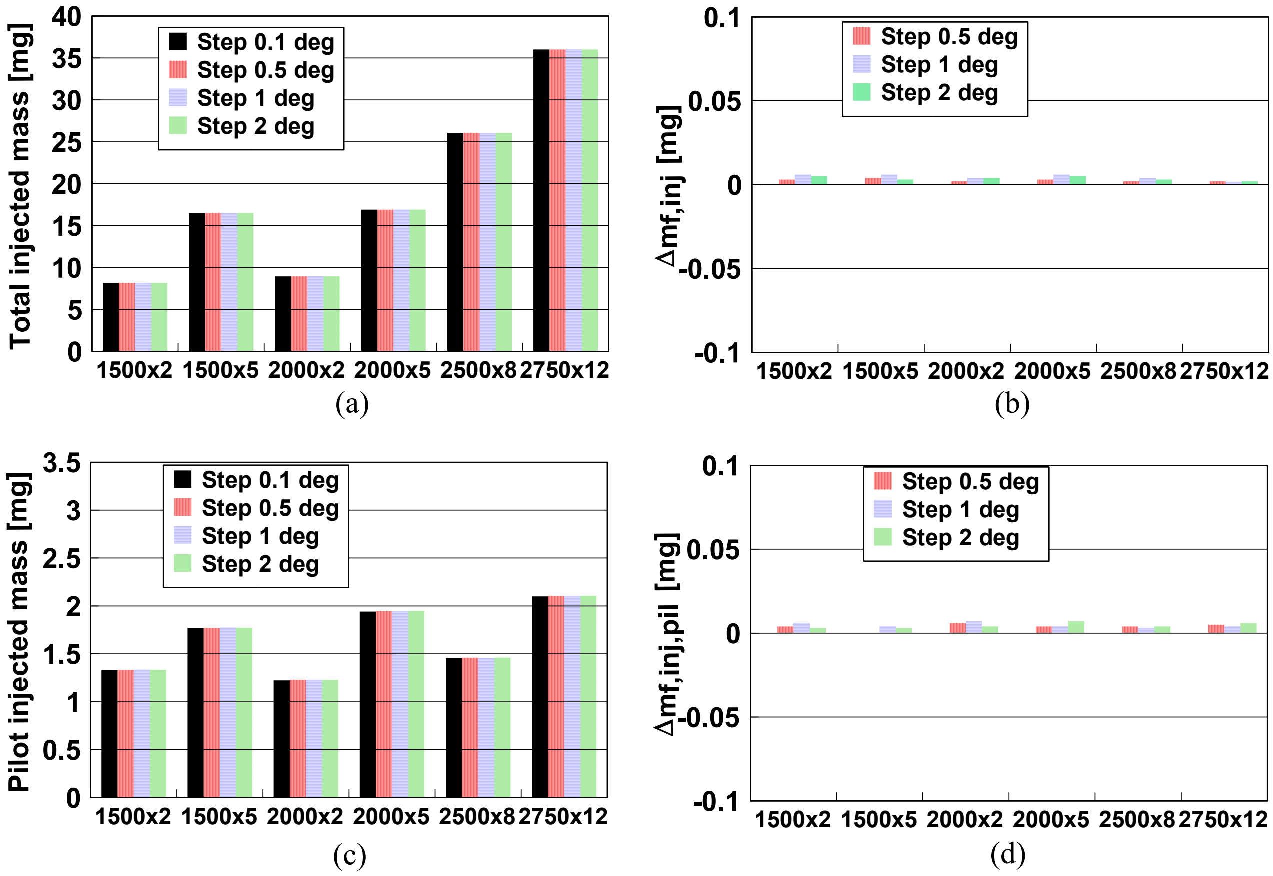

Figure 16 – Effect of the crank angle step used for integration on the estimated total and pilot injected quantities. The differences with respect to the case at 0.1 deg are also reported

(b, d).

The analysis shows that the procedure is very robust with respect to the crank angle step used for integration. It should be specified that the net energy of the charge was calculated according to Eq. (11), using the trapezoidal rule for integration; it has been verified that this integration rule provides a nearly-independent trend of the net energy with respect to the crank angle step used for integration. The computational time that is required for a crank angle step of 2 deg is of the order of 0.3 ms. Therefore, the method can be considered suitable for control-oriented applications.

6. FUTURE WORK

In addition to the injected quantities, the proposed methodology also has the potential of estimating the injection rate curve on the basis of the measured in-cylinder pressure. This can be done by deriving Eq. (28) with respect to time.

An example is reported in Fig. 17 for the 1500x5 and 2000x5 key-points.

In particular, Fig. 17 reports a comparison between the injection rate profiles obtained with the measured in-cylinder pressure (black lines) and the experimental ones (dotted red lines).

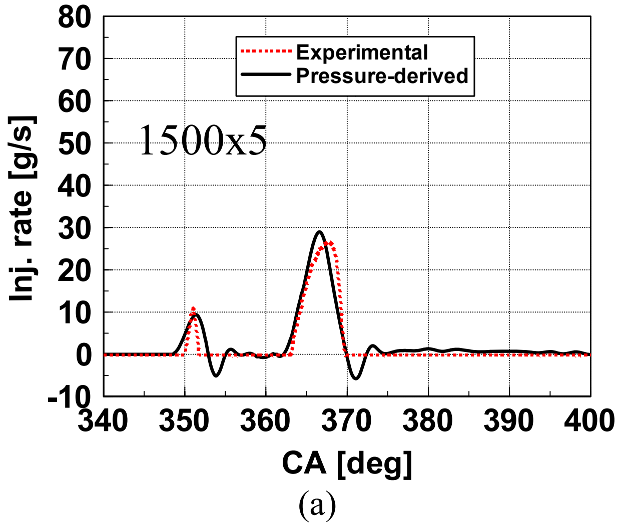

Figure 17 – Comparison between the pressure-derived injection rate profiles and the experimental ones for the 1500x5 and 2000x5 key-points.

It should be noted that the evaluation of the shape of the injection rate is quite good for the 1500x5 key-point, while it shows a double-peak characteristic for the main injection of the 2000x5 key-point. The accuracy of the prediction of the injection rate depends exclusively on the capability of the heat release model to correctly reproduce the HRR shape on the basis of the injection rate profile. It can therefore be observed, in Fig. 17, that the accumulated fuel mass approach (i.e., Eq. (1)) provides good results if the HRR shape is mainly of the premixed type, but is less accurate if the HRR shape is of the premixed-mixing controlled type (see Fig. 8). The result is that the injection rate shape derived from the in-cylinder pressure reflects the premixed-mixing controlled characteristics of the HRR (see Fig. 17b). A refinement in the prediction of the injection rate shape could be realized by refining the heat release model, using, for example, a crank-angle dependent value of the K_j parameters of Eq. (1). This investigation is currently ongoing.

Moreover, the applicability of the proposed method to highly premixed combustion modes, such as PCCI (Premixed Charge Compression Ignition) should also be verified.

7. CONCLUSION

A new methodology has been developed to estimate injected fuel quantities on the basis of the measured in-cylinder pressure in multiple injection DI diesel engines.

The method is based on the inversion of a predictive combustion model that was previously developed by the authors, and which is based on the accumulated fuel mass approach.

A sensitivity analysis has been carried out in order to verify the effects of variations in the main input parameters on the calculated injected quantities. It has been found that errors in the estimation of the global heat transfer of ±50J can lead to errors in the estimation of the total injected quantities of about 1 mg/cyc, but the effect on the estimated pilot quantity error is much smaller (below 0.2 mg/cyc). Moreover, errors in the estimation of the isentropic coefficient γ of ±0.05 lead to large errors for both the estimated total injected quantity (of up to 2 mg/cyc) and for the estimated pilot quantity (of up to 1 mg/cycle). It has also been verified that horizontal shift errors on the in-cylinder pressure of ±0.5 deg lead to errors in the estimated total and pilot quantities of up to 1 mg/cyc and 0.5 mg/cyc, respectively, and vertical shift errors on the in-cylinder pressure of ±0.5 bar lead to errors in the estimated total quantity of up to 0.8 mg/cyc, while the impact on the pilot quantity estimation error is negligible.

An uncertainty analysis has been carried out on the basis of the previous results. It has been verified that the proposed method is robust when used to estimate the injected quantity of the pilot pulses, as the average uncertainty is of the order of 0.15 mg. The average uncertainty in the prediction of the total injected quantity is of the order of 0.9 mg, and depends mainly on the accuracy of the evaluation of the heat transfer of the charge with the walls.

It has also been shown that the method is suitable for evaluating cycle-by-cycle variations of the injected quantities, provided that the input pressure is filtered. However, it has been verified that the use of the raw in-cylinder pressure allows the average injected quantities to be estimated.

Finally, the approach is characterized by a very low computational time, that is, of the order of 0.3 ms, when the elaboration is run on a PC and a crank angle integration step of 2 deg is used, and is therefore suitable for control-oriented applications.

ACKNOWLEDGMENTS

GMPT-E is kindly acknowledged for the technical support in the activity.

REFERENCES

[1] Vanegas A, Won H, Felsch C, Gauding M. et al. Experimental Investigation of the Effect of Multiple Injections on Pollutant Formation in a Common-Rail DI Diesel Engine. SAE Technical Paper 2008-01-1191, 2008, doi:10.4271/2008-01-1191.

[2] Thurnheer T, Edenhauser D, Soltic P, Schreiber D, Kirchen P, Sankowski A. Experimental investigation on different injection strategies in a heavy-duty diesel engine: Emissions and loss analysis. Energ Convers Manage 2011; 52(1):457-467. doi: 10.1016/j.enconman.2010.06.074

[3] Catania AE, d'Ambrosio S, Ferrari A, Finesso R, Spessa E, Avolio G, Rampino V. Experimental Analysis of Combustion Processes and Emissions in a 2.0L Multi-Cylinder Diesel Engine Featuring a New Generation Piezo-Driven Injector. SAE Technical Paper 2009-24-0040, 2009, doi: 10.4271/2009-24-0040.

[4] Catania AE, Ferrari A., Manno M, Spessa E. Experimental Investigation of Dynamics Effects on Multiple-Injection Common Rail System Performance. J. Eng. Gas Turbines Power 2008; 130(3): 032806-1-032806-13. doi: 10.1115/1.2835353.

[5] Catania AE, Ferrari A., Spessa E. Numerical-Experimental Study and Solutions to Reduce the Dwell-Time Threshold for Fusion-Free Consecutive Injections in a Multijet Solenoid-Type CR System. J Eng Gas Turbine Power 2008; 131(2): 022804-1-022804-14. doi: 10.1115/1.2938394.

[6] D'Ambrosio S, Ferrari A. Diesel Injector Coking: Optical-Chemical Analysis of Deposits and Influence on Injected Flow-rate, Fuel Spray and Engine Performance. J Eng Gas Turbine Power 2012; 134(6): 062801-1-062801-14. doi: 10.1115/1.4005991.

[7] Papagiannakis RG, Hountalas DT, Rakopoulos CD. Theoretical study of the effects of pilot fuel quantity and its injection timing on the performance and emissions of a dual fuel diesel engine. Energ Convers Manage 2007; 48(11):2951-2961. doi: 10.1016/j.enconman.2007.07.003

[8] Finesso R, Misul DA, Spessa E. Development and Validation of a Semiempirical Model for the Estimation of Particulate Matter in Diesel Engines. Energ Convers Manage 2014; 84:374-389. doi: 10.1016/j.enconman.2014.04.053.

[9] Ponti F, Corti E, Serra G, De Cesare M. Common Rail Multi-Jet Diesel Engine Combustion Model Development for Control Purposes. SAE Technical Paper 2007-01-0383, 2007. doi:10.4271/2007-01-0383.

[10] Ponti F, Ravaglioli V, Moro D, Serra G. MFB50 On-Board Evaluation Based on a Zero-Dimensional ROHR Model. SAE Technical Paper 2011-01-1420, 2011. doi:10.4271/2011-01-1420.

[11] Chmela FG, Orthaber GC. Rate of Heat Release Prediction for Direct Injection Diesel Engines Based on Purely Mixing Controlled Combustion. SAE Technical Paper 1999-01-0186, 1999. doi:10.4271/1999-01-0186.

[12] Egnell R. A Simple Approach to Studying the Relation between Fuel Rate, Heat Release Rate and NO Formation in Diesel Engines. SAE Technical Paper 1999-01-3548, 1999. doi:10.4271/1999-01-3548.

[13] Catania AE, Finesso R, Spessa E. Predictive Zero-Dimensional Combustion Model for DI Diesel Engine Feed-Forward Control. Energ Convers Manage 2011; 52(10):3159–3175, doi: 10.1016/j.enconman.2011.05.003.

[14] Catania AE, Finesso R, Spessa E, Catanese A, Landsmann G. Combustion Prediction by a Low-Throughput Model in Modern Diesel Engines. SAE Int J Engines 2011; 4(1): 2106-2123. doi: 10.4271/2011-01-1410.

[15] Catania AE, Finesso R, Spessa E. Assessment of a Low-Throughput Predictive Model for Indicated Cycle, Combustion Noise and NOx Calculation in Diesel Engines in Steady-State and Transient Operations. ICES2012-81094, Proceedings of the ASME 2012 Internal Combustion Engine Division Spring Technical Conference, May 6-9, 2012, Torino, Italy. doi: 10.1115/ICES2012-81094.

[16] Arcidiacono M, Baratta M, Finesso R, Kheshtinejad H, Misul D, Spessa E, Yang Y. Use of an Innovative Predictive Heat Release Model Combined to a 1D Fluid-Dynamic Model for the Simulation of a Heavy Duty Diesel Engine. SAE Int. J. Engines 2013; 6(3):1566-1579. doi:10.4271/2013-24-0012.

[17] Alfieri V, Conte G, Finesso R, Spessa E, Yang Y. HRR and MFB50 Estimation in a Euro 6 Diesel Engine by means of Control-Oriented Predictive Models. SAE Int. J. Engines 8(3):1055-1068, 2015, doi:10.4271/2015-01-0879.

[18] Guido C, Beatrice C, Di Iorio S., Napolitano P et al. Assessment of Closed-Loop Combustion Control Capability for Biodiesel Blending Detection and Combustion Impact Mitigation for an Euro5 Automotive Diesel Engine. SAE Technical Paper 2011-01-1193, 2011, doi:10.4271/2011-01-1193.

[19] Schmid U, Seidel H. Study on an injection quantity sensor. I: Evaluation of the integration procedure. Journal of Micromechatronics 2005; 3(1):15 – 32. doi: 10.1163/156856305323383892.

[20] Schmid U, Seidel H. Study on an injection quantity sensor. II: Evaluation of the sensing element. Journal of Micromechatronics 2005; 3(1):33 – 50. doi: 10.1163/156856305323383900.

[21] Finesso R, Spessa E. Ignition delay prediction of multiple injections in diesel engines. Fuel 2014; 119(1):170-190. doi: 10.1016/j.fuel.2013.11.040.

[22] D'Ambrosio S, Finesso R, Spessa E. Calculation Of Mass Emissions, Oxygen Mass Fraction And Thermal Capacity Of The Inducted Charge In SI And Diesel Engines From Exhaust And Intake Gas Analysis. Fuel 2011; 90(1):152–166, doi: http://dx.doi.org/10.1016/j.fuel.2010.08.025.

[23] Catania AE, Finesso R, Spessa E. Real-Time Calculation of EGR Rate and Intake Charge Oxygen Concentration for Misfire Detection in Diesel Engines. SAE Technical Paper 2011-24-0149, 2011. doi: 10.4271/2011-24-0149.

[24] Heywood JB. Internal Combustion Engine Fundamentals. McGraw-Hill, New York, 1988.

[25] Finesso R, Spessa E. A Real Time Zero-Dimensional Diagnostic Model for the Calculation of In-Cylinder Temperatures, HRR and Nitrogen Oxides in Diesel Engines. Energ Convers Manage 2014; 79:498-510. doi: 10.1016/j.enconman.2013.12.045.

[26] Woschni G. A Universally Applicable Equation for the Instantaneous Heat Transfer Coefficient in the Internal Combustion Engine. SAE Technical Paper 670931, 1967, doi: 10.4271/670931.

[27] Baratta M, d'Ambrosio S, Spessa E, Vassallo A. Cycle-Resolved Detection of Combustion Start in SI Engines by Means of Different In-Cylinder Pressure Data Reduction Techniques. ASME 2006 Internal Combustion Engine Division Spring Technical Conference (ICES2006), doi: 10.1115/ICES2006-1367.

[28] ISO/IEC GUIDE 98-3:2008(E).

[29] Rocco V. Dynamic T.D.C. and Thermodynamic Loss Angle Measurement in a D. I. Diesel Engine. SAE Technical Paper 851546, 1985, doi:10.4271/851546